J. Fluid Mech. (2014), *vol.* 742, *pp* 664–700. © Cambridge University Press 2014
doi:10.1017/jfm.2014.2

Steady-state resonance of multiple wave interactions in deep water

Zeng Liu[1] **and Shi-Jun Liao**[1,2,3,†]

[1]State Key Laboratory of Ocean Engineering, School of Naval Architecture, Ocean and Civil Engineering, Shanghai Jiao Tong University, Shanghai 200240, PR China

[2]Key Laboratory of Education-Ministry in Scientific Computing, Department of Mathematics, Shanghai Jiaotong University, Shanghai 200240, PR China

[3]Nonlinear Analysis and Applied Mathematics Research Group (NAAM), King Abdulaziz University (KAU), Jeddah, Saudi Arabia

(Received 26 January 2013; revised 8 November 2013; accepted 24 December 2013; first published online 24 February 2014)

The steady-state resonance of multiple surface gravity waves in deep water was investigated in detail to extend the existing results due to Liao (*Commun. Nonlinear Sci. Numer. Simul.*, vol. 16, 2011, pp. 1274–1303) and Xu *et al.* (*J. Fluid Mech.*, vol. 710, 2012, pp. 379–418) on steady-state resonance from a quartet to more general and coupled resonant quartets, together with higher-order resonant interactions. The exact nonlinear wave equations are solved without assumptions on the existence of small physical parameters. Multiple steady-state resonant waves are obtained for all the considered cases, and it is found that the number of multiple solutions tends to increase when more wave components are involved in the resonance sets. The topology of wave energy distribution in the parameter space is analysed, and it is found that the steady-state resonant waves indeed form a continuum in the parameter space. The significant roles of the near-resonance and nonlinearity were also revealed. It is found that all of the near-resonant components as a whole contain more and more wave energy, as the wave patterns tend from two dimensions to one dimension, or as the nonlinearity of the steady-state resonant wave system increases. In addition, the linear stability of the steady-state resonant waves is analysed. It is found that the steady-state resonant waves are stable, as long as the disturbance does not resonate with any components of the basic wave. All of these findings are helpful to enrich and deepen our understanding about resonant gravity waves.

Key words: surface gravity waves, waves/free-surface flows

1. Introduction

Work on water wave resonance was pioneered by Phillips (1960), who found that the amplitude of a tertiary component grows linearly with time when the resonance condition is satisfied. This flux of potential energy from one wavenumber to another was verified by Longuet-Higgins (1962), who also suggested an experiment to detect

† Email address for correspondence: sjliao@sjtu.edu.cn

the tertiary wave, which was done later by Longuet-Higgins & Smith (1966) and McGoldrick *et al.* (1966). Besides these, the dynamical analysis for a single resonant quartet was considered by Benney (1962) and Bretherton (1964), who concluded that exact solutions in terms of Jacobi elliptic functions may exist. At the same time, the nonlinear resonant interaction of waves in a random sea was considered by (Hasselmann 1962, 1963*a*,*b*). For more details about the early works, please refer to the monographs (Phillips 1977; Craik 1985; Komen *et al.* 1996; Young 1999) and retrospective articles (Phillips 1981; Yuen & Lake 1982; Hammack & Henderson 1993; Dias & Kharif 1999).

Nowadays, it is well known that resonant or near-resonant interactions are the only interactions that affect wave amplitudes to a significant extent (Grimshaw 2005). Let $\boldsymbol{k}_i$ denote the wavenumber, $\omega_i = \sqrt{g|\boldsymbol{k}_i|}$ the linear frequency and g the gravitational acceleration, respectively. Once the resonance criterion found by Phillips (1960), i.e.

$$\boldsymbol{k}_1 \pm \boldsymbol{k}_2 \pm \boldsymbol{k}_3 \pm \boldsymbol{k}_4 = 0, \quad \omega_1 \pm \omega_2 \pm \omega_3 \pm \omega_4 = 0, \tag{1.1}$$

is satisfied by wave components with very small amplitudes a_i, the resonance mechanism is triggered and the energy exchange among these components begins. Usually, the amplitudes a_i of each component in the resonant set are mostly not constants but keep changing with time and so do the corresponding actual amplitude-dependent frequencies σ_i. In some cases, the recurrence of the energy exchange may happen for large times. For a Stokes wave, the side bands associated with it grow exponentially in the initial time, as shown in Benjamin & Brooke (1967); the process responsible for this is believed to be controlled by near-resonant four-wave interaction (Janssen 2003). After long-time evolution, the phenomenon of Fermi–Pasta–Ulam recurrence may occur in a two-dimensional wave field (Yuen & Lake 1982).

As it was believed that the wave amplitude a_i involved in resonance usually changes over time, most researchers focused on the time evolution of resonant wave systems after the work of Phillips (1960) and Hasselmann (1962). They solved different wave model equations from the point of view of initial/boundary-value problems. The so-called steady-state resonant waves correspond to such a state in which all of the amplitudes a_i, the wavenumbers $\boldsymbol{k}_i$ and the actual frequencies σ_i of the resonant wave system are constant, i.e. independent of time, so that the spectrum of wave energy is also independent of time, too. In this paper, we focus on seeking steady-state resonant waves with constant wave amplitudes a_i, wavenumbers $\boldsymbol{k}_i$ and actual frequencies σ_i such that no wave energy is exchanged between different wave components.

Owing to nonlinear effects, the actual wave frequencies σ_i are often slightly different from the linear ones ω_i. As emphasized by Madsen & Fuhrman (2006), it is generally necessary to include the amplitude dispersion, to fully satisfy the nonlinear resonance condition

$$\boldsymbol{k}_1 \pm \boldsymbol{k}_2 \pm \boldsymbol{k}_3 \pm \boldsymbol{k}_4 = 0, \quad \sigma_1 \pm \sigma_2 \pm \sigma_3 \pm \sigma_4 = 0. \tag{1.2}$$

Note that each actual frequency σ_i in (1.2) depends on all of the amplitudes in the wave system. Therefore, a combination of constant amplitudes a_i is required so as to keep the actual frequencies σ_i not only constant but also satisfying the nonlinear resonance condition (1.2) all the time.

As a first step to consider the nonlinear effects on the steady-state resonance waves, we assume that

$$\sigma_1/\omega_1 \equiv \sigma_2/\omega_2 \equiv \sigma_3/\omega_3 \equiv \sigma_4/\omega_4 = \varepsilon, \tag{1.3}$$

where ε is a constant larger than 1, so that both the linear resonance condition (1.1) and the nonlinear ones (1.2) are satisfied at the same time. However, it should be emphasized here that such an assumption is not absolutely necessary by means of the homotopy analysis method (HAM): only the nonlinear condition (1.2) must be satisfied, but the linear one (1.1) is unnecessary, as mentioned in the conclusion of this paper.

Recently, based on the HAM (Liao 1992, 2003, 2012, 2013), Liao (2011) investigated such a steady-state resonance quartet in deep water, and found that multiple steady-state resonance waves exist for the following quartet:

$$2\boldsymbol{k}_1 - \boldsymbol{k}_2 = \boldsymbol{k}_3, \quad 2\omega_1 - \omega_2 = \omega_3, \quad 2\sigma_1 - \sigma_2 = \sigma_3. \tag{1.4}$$

The existence of such steady-state resonant wave systems in water of finite depth has been confirmed by Xu *et al.* (2012). Besides, using a numerical method from the Zakharov equation, Xu *et al.* (2012) obtained qualitatively identical conclusions with that from the fully nonlinear equations by means of the HAM.

However, in both Liao (2011) and Xu *et al.* (2012), only a single special resonant quartet (1.4) is investigated. A single resonant quartet is not sufficiently general, since a system that admits one resonant set of waves often admits many resonant sets simultaneously (Hammack & Henderson 1993). Therefore, waves often interact in coupled sets so that multiple and coupled resonances need to be considered. Also, the role of higher-order nonlinearities in the evolution of random wave fields could be dynamically important (Annenkov & Shrira 2006). The role of the higher-order interaction in the steady-state resonant waves is still an open problem.

In this work, our objective is first to answer some of the above questions, i.e. to investigate the steady-state resonant waves for more general sets in deep water. Then, in order to demonstrate the physical implications of the steady-state resonant waves, we study the topology of the energy distribution in the parameter space. Finally, we investigate numerically the linear stability of steady-state resonance waves.

An outline of this paper is as follows. In § 2, the governing equations and a brief description of the solution procedures are presented (the detailed mathematical formulas are given in the appendix). The extension has been carried out in three aspects: one towards the general resonant quartet in § 3.1; another towards the multiple and coupled resonant quartets in § 3.2; and the third towards the high-order resonant set, a sextet, in § 3.3. The topology of the steady-state resonance waves for a quartet and sextet are shown in § 4.1 and § 4.2, respectively. The linear stability analysis of a quartet is shown in § 5. The conclusions and discussions are given in § 6.

2. The mathematical description

2.1. *Governing equations*

With the fluid motion assumed to be irrotational, a velocity potential $\phi(x, y, z, t)$ can be defined, where t indicates time and (x, y, z) represents the usual Cartesian coordinate system, in which (x, y) defines a horizontal plane located at the mean water level and z is measured vertically upwards. Then we have the velocity $\boldsymbol{u} = (u, v, w) = \nabla\phi$, where $\nabla = (\partial_x, \partial_y, \partial_z)$. Under the assumption of inviscid and incompressible fluid, and without surface tension, the governing equation requires

$$\nabla^2\phi = 0, \tag{2.1}$$

subject to the kinematic and dynamic conditions on the unknown free surface $z = \eta(x, y, t)$,

$$\frac{\partial^2\phi}{\partial t^2} + g\frac{\partial\phi}{\partial z} + \frac{\partial(\boldsymbol{u}^2)}{\partial t} + \boldsymbol{u}\cdot\nabla\left(\frac{1}{2}\boldsymbol{u}^2\right) = 0, \tag{2.2}$$

$$g\eta + \frac{\partial\phi}{\partial t} + \frac{1}{2}\boldsymbol{u}^2 = 0, \tag{2.3}$$

respectively, and the impermeable condition at infinite depth,

$$\frac{\partial\phi}{\partial z} = 0, \quad \text{as} \quad z \to -\infty. \tag{2.4}$$

The above fully nonlinear wave equations with the resonance criteria (1.1) and (1.2) are solved by means of the HAM, as shown below.

2.2. *Solution formulas*

Note that our objective is to find the steady-state resonant waves governed by (2.1)–(2.4) under the resonance criteria (1.1) and (1.2). As mentioned above, Liao (2011) and Xu *et al.* (2012) found the steady-state waves of a single resonant quartet in water of deep and finite depths, respectively, and Xu *et al.* (2012) qualitatively verified their conclusions by means of the Zakharov equation.

Consider the nonlinear interaction of a wave system consisting of κ primary progressive waves, with $\boldsymbol{k}_n$ denoting the wavenumber and σ_n the actual frequency, respectively. For steady-state wave systems, all of the wave amplitudes a_i, the wavenumbers $\boldsymbol{k}_i$ and the actual wave frequencies σ_i are constant, i.e. independent of time. Therefore, the original initial/boundary-value problem (2.1)–(2.4) can be transformed into a boundary-value one by defining a new variable such as

$$\xi_i = \boldsymbol{k}_i\cdot\boldsymbol{r} - \sigma_i t, \quad i = 1, 2, \ldots, \kappa, \tag{2.5}$$

where $\boldsymbol{r} = x\boldsymbol{i} + y\boldsymbol{j}$. In the new coordinate system $(\xi_1, \xi_2, \ldots, \xi_\kappa, z)$, the governing equation (2.1) becomes

$$\sum_{i=1}^{\kappa}\sum_{j=1}^{\kappa}\boldsymbol{k}_i\cdot\boldsymbol{k}_j\frac{\partial^2\phi}{\partial\xi_i\partial\xi_j} + \frac{\partial^2\phi}{\partial z^2} = 0, \tag{2.6}$$

subject to two boundary conditions on the unknown free surface $z = \eta(\xi_1, \xi_2, \ldots, \xi_\kappa)$,

$$\begin{aligned}\mathcal{N}_1[\phi] = {} & \sum_{i=1}^{\kappa}\sum_{j=1}^{\kappa}\sigma_i\sigma_j\frac{\partial^2\phi}{\partial\xi_i\partial\xi_j} + g\frac{\partial\phi}{\partial z} - 2\sum_{i=1}^{\kappa}\sigma_i\frac{\partial f}{\partial\xi_i} + \sum_{i=1}^{\kappa}\sum_{j=1}^{\kappa}\boldsymbol{k}_i\cdot\boldsymbol{k}_j\frac{\partial\phi}{\partial\xi_i}\frac{\partial f}{\partial\xi_j} \\ & + \frac{\partial\phi}{\partial z}\frac{\partial f}{\partial z} = 0,\end{aligned} \tag{2.7}$$

$$\mathcal{N}_2[\eta, \phi] = \eta - \frac{1}{g}\left(\sum_{i=1}^{\kappa}\sigma_i\frac{\partial\phi}{\partial\xi_i} - f\right) = 0, \tag{2.8}$$

and also the bottom condition,

$$\frac{\partial\phi}{\partial z} = 0, \quad \text{as} \quad z \to -\infty, \tag{2.9}$$

where

$$f = \frac{1}{2}\left[\sum_{i=1}^{\kappa}\sum_{j=1}^{\kappa} \boldsymbol{k}_i \cdot \boldsymbol{k}_j \frac{\partial \phi}{\partial \xi_i}\frac{\partial \phi}{\partial \xi_j} + \left(\frac{\partial \phi}{\partial z}\right)^2\right], \tag{2.10}$$

and $\mathcal{N}_1$ and $\mathcal{N}_2$ are the corresponding nonlinear differential operators. Note that a nonlinear boundary-value problem often has multiple solutions. In fact, we indeed obtain the multiple solutions of the above equations for the steady-state resonant waves, as shown below.

Since the steady-state solution means that there is no exchange of wave energy between different wave components, in other words, all the physical quantities related to the wave systems are constant, the steady-state wave elevation $\eta(\xi_1, \xi_2, \ldots, \xi_\kappa)$ can be expressed by

$$\eta = \sum_{m_1=0}^{+\infty}\sum_{m_2=-\infty}^{+\infty}\cdots\sum_{m_\kappa=-\infty}^{+\infty} C^{\eta}_{m_1,m_2,\ldots,m_\kappa}\cos(m_1\xi_1 + m_2\xi_2 + \cdots + m_\kappa\xi_\kappa), \tag{2.11}$$

where $C^{\eta}_{m_1,m_2,\ldots,m_\kappa}$ is a constant to be determined later. According to the linear governing equation (2.6), the linear terms in the dynamic free surface boundary condition (2.8) and the bottom boundary condition (2.9), the velocity potential $\phi(\xi_1, \xi_2, \ldots, \xi_\kappa, y)$ should be in the form

$$\phi = \sum_{m_1=0}^{+\infty}\sum_{m_2=-\infty}^{+\infty}\cdots\sum_{m_\kappa=-\infty}^{+\infty} C^{\phi}_{m_1,m_2,\ldots,m_\kappa}\Psi_{m_1,m_2,\ldots,m_\kappa}, \tag{2.12}$$

with the definition

$$\Psi_{m_1,m_2,\ldots,m_\kappa} = \sin\left(\sum_{i=1}^{\kappa} m_i\xi_i\right)\exp\left(\left|\sum_{i=1}^{\kappa} m_i\boldsymbol{k}_i\right| z\right), \tag{2.13}$$

where $C^{\phi}_{m_1,m_2,\ldots,m_\kappa}$ is a constant to be determined later. Note that the linear governing equation (2.6) and the bottom boundary condition (2.9) are automatically satisfied by (2.12). Thus, the unknown coefficients $C^{\eta}_{m_1,m_2,\ldots,m_\kappa}$ and $C^{\phi}_{m_1,m_2,\ldots,m_\kappa}$ are determined by the two nonlinear boundary conditions (2.7) and (2.8) on the unknown free surface $z = \eta(\xi_1, \xi_2, \ldots, \xi_\kappa)$.

2.3. *Solution procedures*

From the mathematical viewpoint, it is difficult to find the multiple solutions of the nonlinear boundary-value problem governed by (2.6) to (2.9) under the resonance criteria (1.1) and (1.2). Besides, it is well known that multiple solutions are hardly ever found by means of numerical techniques.

Liao (2011) and Xu *et al.* (2012) successfully applied the HAM (Liao 1992, 2012) to gain the multiple solutions of a special steady-state resonance quartet in water of deep and finite depth, respectively. The HAM is an analytic approximation method for highly nonlinear problems. First, the HAM is independent of any small/large physical quantities. Besides, different from all other analytic approximation methods, the HAM provides a convenient way to guarantee the convergence of solution series. In addition, the HAM logically contains some other non-perturbation techniques such as the Lyapunov artificial small parameter method, the famous Adomian decomposition

method (ADM) and so on. Owing to these advantages, the HAM has been successfully applied to solve lots of nonlinear problems in science, engineering and finance, as illustrated by Liao (2012).

Following Liao (2011) and Xu *et al.* (2012), we solve the above nonlinear boundary-value problem to consider coupled and more general resonant sets. For the sake of simplicity, a brief description of the solution procedure in the framework of the HAM is provided in appendix A. It is an extension of the work by Liao (2011) from two primary wave components to multiple primary wave components, with the major difference being the choice of the initial guess. For multiple resonances, all the resonant wave components are to be considered in the initial guess as described in appendix A. For wave resonances caused by high-order wave interactions, additional trivial wave components need to be considered, as shown in the next section.

Note that Xu *et al.* (2012) verified their analytical results by means of the Zakharov equation and a numerical method. In this paper, in order to further verify the correctness of the results obtained by the HAM, the collocation method (Okamura 1996) is applied. For the sake of simplicity, a brief description of it is given in appendix B.

3. General resonant sets

From now on, let us focus on the physical meanings of the mathematical solutions of the nonlinear boundary-value problem mentioned above. For the detailed mathematics, please refer to appendices A and B.

Owing to the nature of the dispersion relation of surface gravity waves, the lowest-order resonance belongs to the four-wave resonance, which controls the evolution of the wave amplitudes (Grimshaw 2005). In this section, the general resonant quartet is considered first in § 3.1. Then a resonance cluster made by combining three single resonant quartets is investigated in § 3.2. Finally a resonant sextet that is generated by higher-order interactions is dealt with in § 3.3.

3.1. *General resonant quartets*

Without loss of generality, we consider wavevectors satisfying the following interaction condition:

$$\boldsymbol{k}_1 + \boldsymbol{k}_2 = \boldsymbol{k}_3 + \boldsymbol{k}_0 = (2, 0), \tag{3.1}$$

where $\boldsymbol{k}_i$ denotes the primary wave component and $\boldsymbol{k}_0$ represents the resonant one. The corresponding linear resonance condition is

$$|\boldsymbol{k}_1|^{1/2} + |\boldsymbol{k}_2|^{1/2} = |\boldsymbol{k}_3|^{1/2} + |\boldsymbol{k}_0|^{1/2} = C, \tag{3.2}$$

where the parameter C controls the path of the resonance curves. Note that, for other sign combinations of the four wave components in the resonance condition, no solution has been found (Phillips 1977). According to the interaction condition (3.1), wavevectors are defined as

$$\boldsymbol{k}_1 = (k_{1x}, k_{1y}), \quad \boldsymbol{k}_2 = (2 - k_{1x}, -k_{1y}), \tag{3.3}$$

$$\boldsymbol{k}_3 = (k_{3x}, k_{3y}), \quad \boldsymbol{k}_0 = (2 - k_{3x}, -k_{3y}). \tag{3.4}$$

Once the parameter C is given, the curves for $\boldsymbol{k}_1$ and $\boldsymbol{k}_3$ can be shown in the (k_x, k_y) wavenumber plane by the resonance condition (3.2), as shown in figure 1 (Phillips 1977).

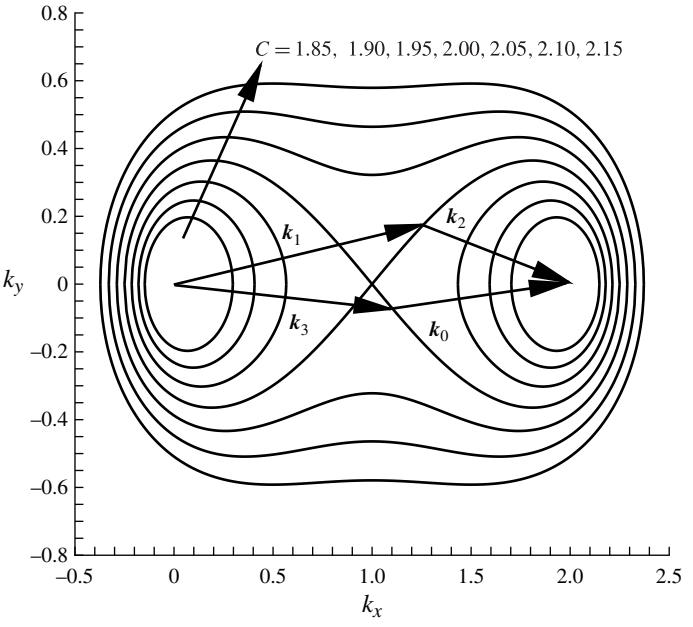

FIGURE 1. Resonant quartets for surface gravity waves. Lines from (0,0) and (2,0) to any pair of points on one such curve determine a resonant quartet.

3.1.1. *The case Q1 of resonant quartet when* $C = 2$

Let us first consider the case $C = 2$, corresponding to the famous 'figure of eight' (Phillips 1960). Note that the special quartet case of $\boldsymbol{k}_1 = \boldsymbol{k}_2$ in (3.1) and (3.2) has been investigated by Liao (2011) for steady-state resonant waves in deep water and by Xu *et al.* (2012) for steady-state resonant waves in water of finite depth. As an extension for the general case $\boldsymbol{k}_1 \neq \boldsymbol{k}_2$, we investigate here $k_{1x} = 1.10$ and $k_{3x} = 1.05$, without loss of generality. The corresponding values of k_{1y} and $k_{3,y}$ are determined by the resonant condition (3.2). The corresponding resonance curve and wavevector configuration are shown in figure 2.

Unlike other analytic approximation methods, the HAM provides great freedom to choose the initial guess for the solution. As mentioned in appendix A, the general forms of the initial guess (A 18) and (A 19) read

$$\eta_0 = 0, \tag{3.5}$$

$$\phi_0 = A_{0,1}\Psi_{1,0,0} + A_{0,2}\Psi_{0,1,0} + A_{0,3}\Psi_{0,0,1} + A_{0,4}\Psi_{1,1,-1}, \tag{3.6}$$

where $A_{0,1}$, $A_{0,2}$, $A_{0,3}$ and $A_{0,4}$ are unknowns, which will be determined later. Substituting the initial guesses into the so-called first-order deformation equation (A 9) in the frame of the HAM, we have

$$\begin{aligned}\bar{\mathcal{L}}\phi_1 &= c_0\Delta_0^{\phi} - \bar{S}_1 \\ &= b_{1,0,0}\sin(\xi_1) + b_{0,1,0}\sin(\xi_2) + b_{0,0,1}b_{1,0,0}\sin(\xi_3) + b_{1,1,0}\sin(\xi_1+\xi_2) \\ &\quad + b_{1,0,1}\sin(\xi_1+\xi_3) + b_{0,1,1}\sin(\xi_2+\xi_3) + b_{1,-1,0}\sin(\xi_1-\xi_2) \\ &\quad + b_{1,0,-1}\sin(\xi_1-\xi_3) + b_{0,1,-1}\sin(\xi_2-\xi_3) + b_{1,1,1}\sin(\xi_1+\xi_2+\xi_3) \\ &\quad + b_{1,-1,1}\sin(\xi_1-\xi_2+\xi_3) + b_{1,1,-1}\sin(\xi_1+\xi_2-\xi_3) + \cdots,\end{aligned} \tag{3.7}$$

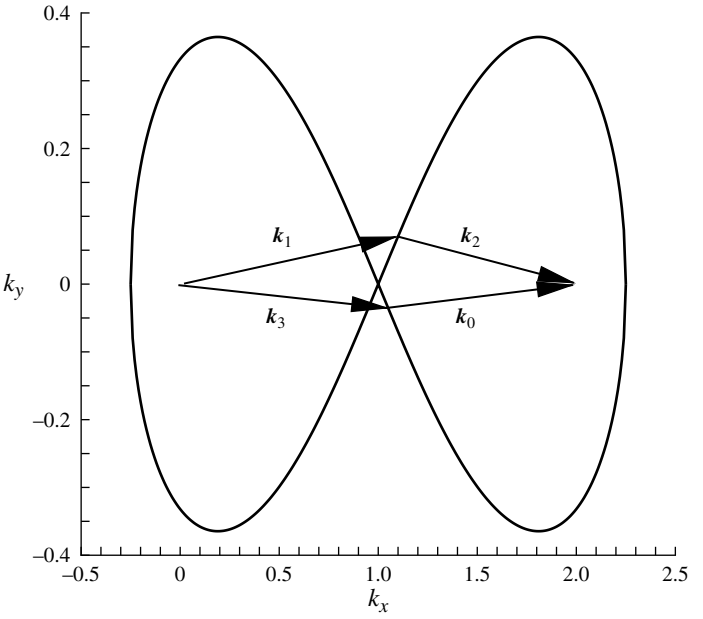

FIGURE 2. Wavevector configuration of a resonant quartet Q1. Specification: $C = 2$, $\boldsymbol{k}_1 = (1.10, 0.070227)$ and $\boldsymbol{k}_3 = (1.05, -0.0352947)$.

where $b_{m,n,l}$ depends on the four unknown coefficients $A_{0,1}$, $A_{0,2}$, $A_{0,3}$ and $A_{0,4}$ in the initial guess (3.6). Owing to the property of the inverse linear operator (A 12), the coefficients of the terms $\sin\xi_1$, $\sin\xi_2$, $\sin\xi_3$ and $\sin(\xi_1 + \xi_2 - \xi_3)$ on the right-hand side of (3.7) must be zero so as to avoid the secular terms. Forcing the coefficients $b_{1,0,0}$, $b_{0,1,0}$, $b_{0,0,1}$ and $b_{1,1,-1}$ to be equal to zero gives the coupled nonlinear algebraic equations:

$$-0.000648788 + 1.47606\,A_{0,1}^2 + 1.63163\,A_{0,2}^2 + 2.56262\,A_{0,3}^2 + 1.89437\,A_{0,4}^2 + 1.62616\,A_{0,2}A_{0,3}A_{0,4}/A_{0,1} = 0, \tag{3.8}$$

$$-0.000531358 + 2.42765\,A_{0,1}^2 + 0.664114\,A_{0,2}^2 + 2.09448\,A_{0,3}^2 + 1.55602\,A_{0,4}^2 + 2.42616\,A_{0,1}A_{0,3}A_{0,4}/A_{0,2} = 0, \tag{3.9}$$

$$-0.000618388 + 2.82013\,A_{0,1}^2 + 1.54666\,A_{0,2}^2 + 1.21825\,A_{0,3}^2 + 1.80773\,A_{0,4}^2 + 1.81121\,A_{0,1}A_{0,2}A_{0,4}/A_{0,3} = 0, \tag{3.10}$$

$$-0.000559564 + 2.54652\,A_{0,1}^2 + 1.40358\,A_{0,2}^2 + 2.20723\,A_{0,3}^2 + 0.816756\,A_{0,4}^2 + 2.2112\,A_{0,1}A_{0,2}A_{0,3}/A_{0,4} = 0. \tag{3.11}$$

Here, each equation has been divided by $A_{0,i}$ to guarantee that $A_{0,i} \neq 0$. This set of nonlinear algebraic equations (3.8)–(3.11) has 48 real solutions, which can be divided into six different groups according to the absolute values as shown in table 1.

It is found that it is the last terms (related to $A_{0,1}A_{0,2}A_{0,3}A_{0,4}/A_{0,i}^2$, $i = 1, 2, 3, 4$) in (3.8)–(3.11) that lead to multiple real solutions of $A_{0,1}$, $A_{0,2}$, $A_{0,3}$ and $A_{0,4}$. Without these terms, only one group of real solutions exists. A detailed investigation shows that these terms are generated by the last two terms in (2.7), in which the potential

Group	$\lvert A_{0,1}\rvert$	$\lvert A_{0,2}\rvert$	$\lvert A_{0,3}\rvert$	$\lvert A_{0,4}\rvert$
1	0.00697277	0.00940638	0.00751135	0.00872688
2	0.0139994	0.00932267	0.00750222	0.00873061
3	0.00691502	0.0188538	0.00754224	0.00873289
4	0.00697889	0.00944319	0.0149749	0.00880325
5	0.00929137	0.0125585	0.0101486	0.0117792
6	0.00699333	0.00941644	0.00757762	0.0173988

TABLE 1. Solutions of the nonlinear algebraic equations (3.8)–(3.11) for the case Q1. Specification: $C = 2$, $\boldsymbol{k}_1 = (1.10, 0.070227)$, $\boldsymbol{k}_3 = (1.05, -0.0352947)$ and $\varepsilon = 1.00003$.

function is of power three. The following manipulation on the initial guess (3.5)–(3.6) shows this procedure more clearly:

$$\begin{aligned}&\frac{\partial}{\partial z}(A_{0,2}\Psi_{0,1,0})\frac{\partial}{\partial z}\left(\frac{\partial}{\partial z}(A_{0,3}\Psi_{0,0,1})\frac{\partial}{\partial z}(A_{0,4}\Psi_{1,1,-1})\right)\Big|_{z=0}\\ &\quad\sim A_{0,2}A_{0,3}A_{0,4}\sin(\xi_2)\sin(\xi_3)\sin(\xi_1+\xi_2-\xi_3)\\ &\quad\sim A_{0,2}A_{0,3}A_{0,4}\sin(\xi_1)+\cdots,\end{aligned} \tag{3.12}$$

which is extracted from the last term in (2.7). Equation (3.12) shows the influence of the triad mutual interaction among the second and third primary and the resonant wave components on the first primary ones, which leads to the last term in (3.8). For all the primary and resonant wave components in the resonant quartet, each one can be affected by the other three through the triad mutual interactions. So, it is due to the cubic nonlinear terms in (2.7) that the triad mutual interaction among the primary and resonant wave components leads to the multiple steady-state resonance waves for the quartet. Note that recognizing the origin of the multiple steady-state resonant waves is the cornerstone for higher-order interactions, as shown in § 3.3.

Once $A_{0,1}$, $A_{0,2}$, $A_{0,3}$ and $A_{0,4}$ are determined, all the terms on the right-hand side of (A 9) and (A 10) in the first-order deformation equation are known. Thus, η_1 can be directly obtained from (A 10) and ϕ_1, say,

$$\phi_1 = \bar{\mathcal{L}}^{-1}[c_0\Delta_0^{\phi} - \bar{S}_1] + A_{1,1}\Psi_{1,0,0} + A_{1,2}\Psi_{0,1,0} + A_{1,3}\Psi_{0,0,1} + A_{1,4}\Psi_{1,1,-1}, \tag{3.13}$$

which also contains the four unknown coefficients $A_{1,1}$, $A_{1,2}$, $A_{1,3}$ and $A_{1,4}$ that can be determined in a similar way at the second-order approximation. For $m \geqslant 1$, the unknown coefficients $A_{m-1,1}$, $A_{m-1,2}$, $A_{m-1,3}$ and $A_{m-1,4}$ and the two unknown functions η_m and ϕ_m can be obtained in a similar way, except that the four unknown coefficients are determined by a set of linear algebraic equations.

Note that, unlike all other approximation methods, the HAM provides us with a convenient way to guarantee the convergence of solution series by introducing the so-called 'convergence-control parameter' c_0. At the mth-order approximation, the optimal approximation is given by the optimal value of the convergence-control parameter c_0 that is determined by minimizing the averaged residual squares.

When $\varepsilon = 1.0003$ in the case Q1, four groups of convergent solutions are obtained and the wave amplitudes of the primary and resonant wave components are listed in table 2. The corresponding wave energy distributions are given in table 3. Here Π

Group	Amplitude of wave components: Primary wave			Resonant wave
	$\lvert C^{\eta}_{1,0,0}\rvert$	$\lvert C^{\eta}_{0,1,0}\rvert$	$\lvert C^{\eta}_{0,0,1}\rvert$	$\lvert C^{\eta}_{1,1,-1}\rvert$
1	0.002909	0.002305	0.002816	0.002480
2	0.005588	0.002467	0.001564	0.002008
4	0.001701	0.002841	0.005490	0.002142
6	0.002356	0.003592	0.002453	0.005104

TABLE 2. Amplitude of wave components $|C^{\eta}_{1,0,0}|$, $|C^{\eta}_{0,1,0}|$, $|C^{\eta}_{0,0,1}|$ and $|C^{\eta}_{1,1,-1}|$ for the case Q1. Specification: $C = 2$, $\boldsymbol{k}_1 = (1.10, 0.070227)$, $\boldsymbol{k}_3 = (1.05, -0.0352947)$ and $\varepsilon = 1.00003$.

Group	Percentage of wave energy distribution (%): Primary wave			Resonant wave
	$\dfrac{\lvert C^{\eta}_{1,0,0}\rvert^2}{\Pi}$	$\dfrac{\lvert C^{\eta}_{0,1,0}\rvert^2}{\Pi}$	$\dfrac{\lvert C^{\eta}_{0,0,1}\rvert^2}{\Pi}$	$\dfrac{\lvert C^{\eta}_{1,1,-1}\rvert^2}{\Pi}$
1	30.38	19.08	28.47	22.07
2	71.30	13.90	5.59	9.21
4	6.33	17.67	65.96	10.04
6	10.98	25.54	11.91	51.56

TABLE 3. Wave energy distribution for different groups of steady-state resonant wave systems for the case Q1. Specification: $C = 2$, $\boldsymbol{k}_1 = (1.10, 0.070227)$, $\boldsymbol{k}_3 = (1.05, -0.0352947)$ and $\varepsilon = 1.00003$.

denotes the total wave energy of the entire wave system,

$$\Pi = \sum_{m_1=0}^{+\infty} \sum_{m_2=0}^{+\infty} \cdots \sum_{m_\kappa=0}^{+\infty} (C^{\eta}_{m_1,m_2,\ldots,m_\kappa})^2. \tag{3.14}$$

For each group in table 2, the resonant wave amplitude is of the same order as that of the three primary ones, which agrees with the conclusions given by Benney (1962), Liao (2011) and Xu *et al.* (2012). Further, the resonant wave components may contain the majority (51.56%) of the total wave energy, the same amount (22.07%) as that of the primary wave component, or only a small amount (9.21%, 10.04%), as shown in group 6, group 1, and groups 2 and 4 of table 3, respectively.

3.1.2. *The case Q2 of resonant quartet when $C < 2$*

It is found that, when $C < 2$, the resonance curve splits from the 'figure of eight' into two symmetrical curves. Without loss of generality, substituting $C = 1.997$, $k_{1x} = 1.20$ and $k_{3x} = 0.88$ into the resonant condition (3.2), and applying only the positive values of k_{1y} and $k_{3,y}$ this time, we get the wavevector configuration as shown in figure 3(*a*). Similarly to the case of $\varepsilon = 1.00003$, it is found that there exist three steady-state resonant waves, and the resonant wave component may contain the majority (78.15%) of the total wave energy, the same amount (34.84%) as that of the primary wave component, or only quite a small amount (0.03%), as shown in group 3, group 2 and group 1 in table 4, respectively. This illustrates the generality of the existence of the multiple steady-state resonant waves.

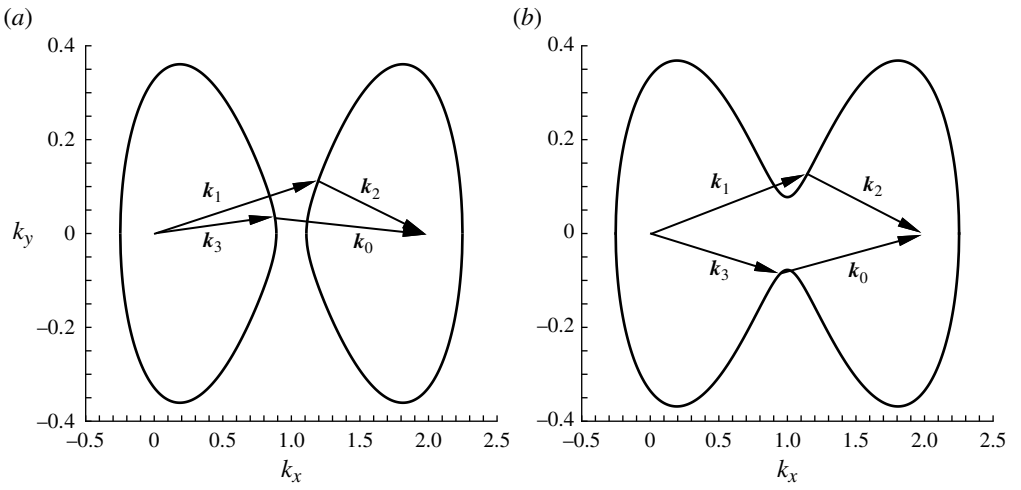

FIGURE 3. Wavevector configuration of two resonant quartets Q2 and Q3. Specification: (*a*) Q2, $\boldsymbol{k}_1 = (1.20, 0.115293)$ and $\boldsymbol{k}_3 = (0.88, 0.0346442)$ when $C = 1.997$; (*b*) Q3, $\boldsymbol{k}_1 = (1.15, 0.12933)$ and $\boldsymbol{k}_3 = (0.95, -0.0850699)$ when $C = 2.003$.

Group	Percentage of wave energy distribution (%) Primary wave		Resonant wave	
	$\frac{\lvert C^{\eta}_{1,0,0}\rvert^2}{\Pi}$	$\frac{\lvert C^{\eta}_{0,1,0}\rvert^2}{\Pi}$	$\frac{\lvert C^{\eta}_{0,0,1}\rvert^2}{\Pi}$	$\frac{\lvert C^{\eta}_{1,1,-1}\rvert^2}{\Pi}$
1	86.93	12.98	0.06	0.03
2	39.65	11.08	14.43	34.84
3	0.94	17.88	3.03	78.15

TABLE 4. Wave energy distribution for different groups of steady-state fully resonant wave systems for case Q2. Specification: $C = 1.997$, $\boldsymbol{k}_1 = (1.20, 0.115293)$, $\boldsymbol{k}_3 = (0.88, 0.0346442)$ and $\varepsilon = 1.00003$.

3.1.3. *The case Q3 of resonant quartet when* $C > 2$

When $C > 2$, the resonance curve merges into a single one. Without loss of generality, substituting $C = 2.003$, $k_{1x} = 1.15$ and $k_{3x} = 0.95$ into the resonant condition (3.2), we get the wavevector configuration for $k_{1y} > 0$ and $k_{3,y} < 0$, as shown in figure 3(*b*). Similarly to the case of $\varepsilon = 1.00003$, it is found that there exist four steady-state resonant waves, and in addition the resonant wave component may contain the majority (67.39%) of the total wave energy, the same amount (28.69%) as that of the primary wave component, or only a small amount (2.31%, 8.60%), as shown in group 4, group 1, and groups 2 and 3 of table 5, respectively. This confirms once again the generality of the existence of the steady-state resonant waves for different values of C in the condition (3.2) for a single resonant quartet.

Note that Liao (2011) and Xu *et al.* (2012) only considered the case $C = 2$ of the condition (3.2) for a single resonant quartet in deep and finite water depth, respectively. So, the above works extend their conclusions to all cases of $C < 2$, $C = 2$ and $C > 2$, and thus reveal the wide generality of the existence of steady-state resonant waves. We

Group	Percentage of wave energy distribution (%)			
	Primary wave			Resonant wave
	$\frac{\lvert C^{\eta}_{1,0,0}\rvert^2}{\Pi}$	$\frac{\lvert C^{\eta}_{0,1,0}\rvert^2}{\Pi}$	$\frac{\lvert C^{\eta}_{0,0,1}\rvert^2}{\Pi}$	$\frac{\lvert C^{\eta}_{1,1,-1}\rvert^2}{\Pi}$
1	33.33	15.97	22.00	28.69
2	78.04	15.91	3.74	2.31
3	7.41	27.39	56.59	8.60
4	4.04	21.56	7.01	67.39

TABLE 5. Wave energy distribution for different groups of steady-state fully resonant wave systems for case Q3. Specification: $C = 2.003$, $\boldsymbol{k}_1 = (1.15,\ 0.12933)$, $\boldsymbol{k}_3 = (0.95,\ -0.0850699)$ and $\varepsilon = 1.00003$.

will extend the same conclusions to multiple and coupled resonant quartets in § 3.2, and even to a resonant sextet in § 3.3.

3.2. *Multiple and coupled resonant quartets*

To further investigate whether or not the steady-state resonant waves exist for more general and complicated configurations, let us consider a wave system made up of three single resonant quartets (case C1):

$$\begin{cases} \boldsymbol{k}_1 + \boldsymbol{k}_2 = \boldsymbol{k}_3 + \boldsymbol{k}_{0,1} = \boldsymbol{k}_4 + \boldsymbol{k}_{0,2} = (2,\ 0), \\ |\boldsymbol{k}_1|^{1/2} + |\boldsymbol{k}_2|^{1/2} = |\boldsymbol{k}_3|^{1/2} + |\boldsymbol{k}_{0,1}|^{1/2} = |\boldsymbol{k}_4|^{1/2} + |\boldsymbol{k}_{0,2}|^{1/2} = 2, \end{cases} \tag{3.15}$$

where $\boldsymbol{k}_i$ denotes the primary wave component, and $\boldsymbol{k}_{0,i}$ represents the resonant ones. All the six harmonics are on the same resonance curve. Without loss of generality, we choose here $\boldsymbol{k}_1 = (1.10,\ 0.070227)$, $\boldsymbol{k}_3 = (1.05,\ -0.0352947)$ and $\boldsymbol{k}_4 = (1.03,\ 0.0212001)$. The corresponding wavevector configuration is shown in figure 4. The geometrical structure becomes more complicated from the case Q1 for a resonant quartet to the case C1 for three coupled quartets, while their external configurations are the same.

Compared to the case Q1 for a single resonant quartet, one more primary wave and one more resonant one had to be considered in the case C1. Thus, we have two more terms in the initial guess for the potential function,

$$\begin{aligned} \phi_0 \ = \ & A_{0,1}\Psi_{1,0,0,0} + A_{0,2}\Psi_{0,1,0,0} + A_{0,3}\Psi_{0,0,1,0} + A_{0,4}\Psi_{0,0,0,1} \\ & + A_{0,5}\Psi_{1,1,-1,0} + A_{0,6}\Psi_{1,1,0,-1}, \end{aligned} \tag{3.16}$$

where $A_{0,i}$ $(1 \leqslant i \leqslant 6)$ are unknown real constant coefficients. Here, we emphasize that in the frame of the HAM we have great freedom to choose the initial guess. Similarly, in the frame of the HAM, these six unknown constant coefficients are determined by avoiding the secular terms of the first-order approximation, which leads to a set of nonlinear algebraic equations of these six unknown coefficients. In the case C1, six groups of steady-state resonant waves are found by means of the HAM. The energy distributions of the six groups are shown in table 6. Note that the wave energy distribution changes dramatically from group to group. The two resonant components together may contain quite a small amount (10.89%) of the total wave energy.

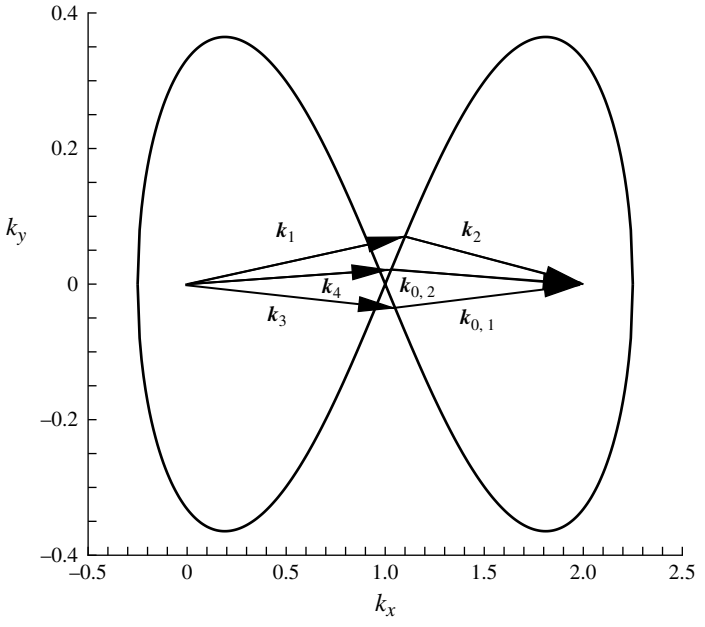

FIGURE 4. Wavevector configuration of coupled resonant quartets C1. Specification: $\boldsymbol{k}_1 = (1.10, 0.070227)$, $\boldsymbol{k}_3 = (1.05, -0.0352947)$ and $\boldsymbol{k}_4 = (1.03, 0.0212001)$.

Group	Percentage of wave energy distribution (%)					
	Primary wave			Resonant wave		
	$\frac{\lvert C^{\eta}_{1,0,0,0}\rvert^2}{\Pi}$	$\frac{\lvert C^{\eta}_{0,1,0,0}\rvert^2}{\Pi}$	$\frac{\lvert C^{\eta}_{0,0,1,0}\rvert^2}{\Pi}$	$\frac{\lvert C^{\eta}_{0,0,0,1}\rvert^2}{\Pi}$	$\frac{\lvert C^{\eta}_{1,1,-1,0}\rvert^2}{\Pi}$	$\frac{\lvert C^{\eta}_{1,1,0,-1}\rvert^2}{\Pi}$
1	45.28	0.51	39.91	3.37	0.87	10.02
2	3.96	7.37	5.52	57.78	8.48	16.89
3	19.57	12.50	18.80	18.80	14.82	15.34
4	47.49	0.21	3.84	2.06	16.83	29.57
5	46.06	0.08	0.49	40.78	12.48	0.11
6	0.001	34.48	9.51	9.07	21.59	25.12

TABLE 6. Wave energy distribution for different groups of steady-state resonant wave systems for case C1. Specification: $\boldsymbol{k}_1 = (1.10, 0.070227)$, $\boldsymbol{k}_3 = (1.05, -0.0352947)$, $\boldsymbol{k}_4 = (1.03, 0.0212001)$ and $\varepsilon = 1.00003$.

This work further confirms the generality of the existence of the steady-state resonant waves for complicated systems with coupled resonant quartets.

3.3. *Resonant sextet*

In this subsection, we study the higher-order nonlinear resonant interactions so as to investigate whether or not the multiple steady-state resonant waves exist for even more complicated systems. Without loss of generality, a resonant sextet in the case $\varepsilon = 1.00001$ is illustrated here.

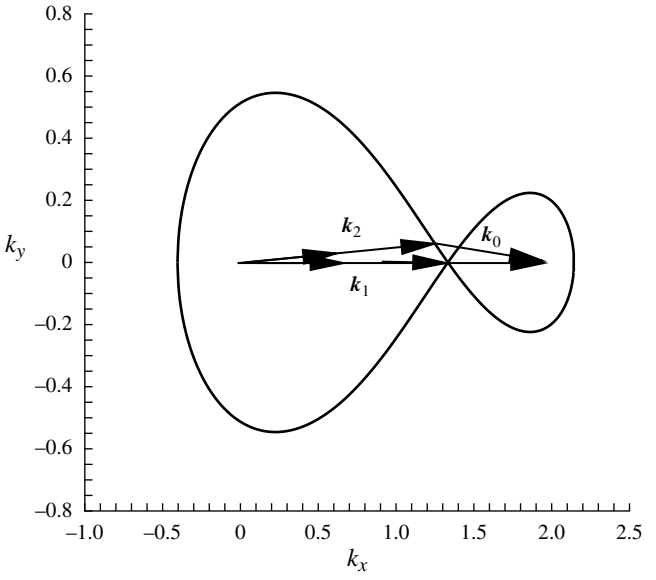

FIGURE 5. Wavevector configuration of one resonant sextet S1. Specification: $\boldsymbol{k}_1 = (0.667, 0)$ and $\boldsymbol{k}_2 = (0.625, 0.0302171)$.

Without loss of generality, let us consider the case S1:

$$\begin{cases} 3\boldsymbol{k}_1 = 2\boldsymbol{k}_2 + \boldsymbol{k}_0 = (2, 0), \\ 3|\boldsymbol{k}_1|^{1/2} = 2|\boldsymbol{k}_2|^{1/2} + |\boldsymbol{k}_0|^{1/2} = \sqrt{6}, \end{cases} \tag{3.17}$$

where $\boldsymbol{k}_1$ and $\boldsymbol{k}_2$ denote the primary wave components and $\boldsymbol{k}_0$ represents the resonant ones, respectively. The corresponding resonance curve is still a 'figure of eight', but the symmetry along the vertical line is broken, as shown in figure 5. Note that $\boldsymbol{k}_1 = (2/3, 0)$ is determined automatically by the resonance condition (3.17). For the second primary wavevector, $\boldsymbol{k}_2 = (0.625, 0.030217)$ is considered here, and the corresponding wavevector configuration is shown in figure 5.

Recall that it is due to the cubic nonlinear terms of the potential function that we could find the multiple steady-state resonant waves. However, the higher-order harmonic $\cos(m\xi_1 + n\xi_2)$ $(|m| + |n| > 3)$ cannot be directly affected by the first-order harmonics $\cos(\xi_1)$ and $\cos(\xi_2)$ within the triad mutual interactions; thus no multiple solutions can be gained if the same kind of initial guess as in a resonant quartet is used. From the mathematical viewpoint, one can add such a tertiary component in the initial guess that the primary and resonant components can be affected through the triad mutual interaction. Fortunately, the HAM indeed provides us with great freedom to choose initial guesses. In the case S1 defined by (3.17), the possible candidates for the tertiary component are $\sin(\xi_1 - 2\xi_2)$, $\sin(2\xi_1 - \xi_2)$ and $\sin(3\xi_1)$. Taking $\sin(\xi_1 - 2\xi_2)$ as an example, the initial guess for the potential function now becomes

$$\phi_0 = A_{0,1}\Psi_{1,0} + A_{0,2}\Psi_{0,1} + A_{0,3}\Psi_{3,-2} + A_{0,4}\Psi_{1,-2}, \tag{3.18}$$

where $A_{0,1}$, $A_{0,2}$, $A_{0,3}$ and $A_{0,4}$ are unknown constant coefficients. Similarly, avoiding the secular terms gives us three nonlinear algebraic equations. These however are

Group	$\lvert A_{0,1}\rvert$	$\lvert A_{0,2}\rvert$	$\lvert A_{0,3}\rvert$	$\lvert A_{0,4}\rvert$
1	0.0149336	0.0163336	0.000128827	0.000193217
2	0.0114729	0.012641	0.00961348	3.544×10^{-7}
3	0.0114245	0.0126743	0.00969989	0.000176524

TABLE 7. Solutions of the nonlinear algebraic equations (3.19)–(3.22) for case S1. Specification: $\boldsymbol{k}_1 = (0.667, 0)$, $\boldsymbol{k}_2 = (0.625, 0.0302171)$ and $\varepsilon = 1.00001$.

not enough, because we have now four unknown coefficients. In addition, since the additional tertiary component is a trivial one, we can force the coefficient of $\sin(\xi_1 - 2\xi_2)$ on the right-hand side of (A 9) in the first-order approximation to be zero. In this way, we get the following four coupled nonlinear algebraic equations:

$$-0.000130801 + 0.197531\,A_{0,1}^2 + 0.326866\,A_{0,2}^2 + 0.568799\,A_{0,3}^2 + 0.269745\,A_{0,4}^2 - 0.134459\,A_{0,4}A_{0,2}^2/A_{0,1} - 0.39717\,A_{0,4}A_{0,3} = 0, \tag{3.19}$$

$$-0.000122769 + 0.371006\,A_{0,1}^2 + 0.153302\,A_{0,2}^2 + 0.534936\,A_{0,3}^2 + 0.252622\,A_{0,4}^2 - 0.307381\,A_{0,4}A_{0,1} = 0, \tag{3.20}$$

$$-0.000147628 + 0.446697\,A_{0,1}^2 + 0.370513\,A_{0,2}^2 + 0.320528\,A_{0,3}^2 + 0.306777\,A_{0,4}^2 - 0.152045\,A_{0,4}A_{1,0}^2/A_{0,3} = 0, \tag{3.21}$$

$$0.00346688 + 0.348341\,A_{0,1}^2 + 0.287563\,A_{0,2}^2 + 0.502895\,A_{0,3}^2 + 0.118288\,A_{0,4}^2 - 0.173814\,A_{0,1}A_{0,2}^2/A_{0,4} - 0.250811\,A_{0,1}^2A_{0,3}/A_{0,4} = 0, \tag{3.22}$$

which has three groups of real solutions, as shown in table 7. Note that, without the tertiary component added in the initial guess, only one solution (corresponding to group 2) can be found.

It is found that there exist three groups of steady-state resonant waves, and the corresponding amplitudes of the primary, resonant and candidate tertiary wave components are given in table 8. Note that the primary and resonant wave components are of the same order in group 2 and group 3, but the amplitude of the resonant wave in group 1 is one order lower than that of the primary ones. Besides, the amplitudes of all the candidate tertiary wave components are much lower than that of the primary and resonant ones (this however is not always the case, as shown in the next section). It is found that, for this resonant sextet, the resonant wave components may contain the majority (52.25%) of the total wave energy, or only a small amount (0.44%), as shown in group 3 and group 1 in table 9, respectively.

Similarly, when the second candidate tertiary component $\sin(2\xi_1 - \xi_2)$ is considered in the initial guess, three groups of real solutions are found for the four corresponding unknown coefficients. These three groups of solutions give exactly the same results as those listed in tables 8 and 9. In addition, when both the first candidate tertiary components $\sin(\xi_1 - 2\xi_2)$ and the second ones $\sin(2\xi_1 - \xi_2)$ are considered in the initial guess, exactly the same three groups of solutions are found. This verifies the validity of our HAM-based approach for the higher-order resonant sextet.

It should be emphasized that not only the primary and resonant wave components but also the trivial ones are considered in the initial guess, so that the primary and resonant wave components can be affected by each other through the triad mutual interaction. In the considered case for a resonant sextet, it is found that the

Group	Amplitude of wave components					
	Primary wave		Resonant wave	Candidates tertiary wave		
	$\lvert C^{\eta}_{1,0}\rvert$	$\lvert C^{\eta}_{0,1}\rvert$	$\lvert C^{\eta}_{3,-2}\rvert$	$\lvert C^{\eta}_{1,-2}\rvert$	$\lvert C^{\eta}_{2,-1}\rvert$	$\lvert C^{\eta}_{3,0}\rvert$
1	0.004181	0.004020	0.000384	0.000038	0.000288	1.037×10^{-8}
2	0.003019	0.002269	0.003510	0.000011	0.000116	3.654×10^{-9}
3	0.003069	0.001899	0.003783	0.000026	0.000214	1.001×10^{-8}

TABLE 8. Amplitude of primary, resonant and candidate tertiary wave components for case S1. Specification: $\boldsymbol{k}_1 = (0.667, 0)$, $\boldsymbol{k}_2 = (0.625, 0.0302171)$ and $\varepsilon = 1.00001$.

Group	Percentage of wave energy distribution (%)		
	Primary wave		Resonant wave
	$\dfrac{\lvert C^{\eta}_{1,0}\rvert^2}{\Pi}$	$\dfrac{\lvert C^{\eta}_{0,1}\rvert^2}{\Pi}$	$\dfrac{\lvert C^{\eta}_{3,-2}\rvert^2}{\Pi}$
1	51.61	47.7	0.44
2	34.27	19.36	46.31
3	34.4	13.18	52.25

TABLE 9. Wave energy distribution for different groups of steady-state resonant wave systems for case S1. Specification: $\boldsymbol{k}_1 = (0.667, 0)$, $\boldsymbol{k}_2 = (0.625, 0.0302171)$ and $\varepsilon = 1.00001$.

amplitudes of the primary and resonant components are much greater than that of the trivial tertiary ones. Besides, the order of the resonant component is not always the same as that of the primary ones. Even so, our HAM-based approach works well, no matter whether the amplitudes of the wave components are of the same order or not. This is mainly because the HAM is entirely independent of small physical parameters. Besides, the HAM provides us with great freedom to choose the initial guess. This kind of freedom relies strongly on the advantage of HAM: it does not need any assumptions about the amplitudes of the wave components.

In summary, using the HAM as a tool, we successfully extended the existence of the multiple steady-state resonant waves in three aspects: from a special, single quartet to more general quartets; or to more complicated wave systems such as coupled resonant quartets; or from the four-wave interactions to the higher-order interactions. In all of the considered cases, there exist multiple steady-state resonant waves, and the number of multiple solutions may increase as more wave components are involved in the resonant sets. Therefore, for a resonance cluster (Kartashova 2010) that contains many resonant sets, lots of steady-state resonant waves should exist.

4. Topology of the steady-state resonance waves

To examine the topology of the steady-state resonant waves in the parameter space, we investigate the energy distribution versus the wavevectors or the dimensionless frequency ε. Both a resonant quartet and a resonant sextet are considered, and the corresponding linear resonance conditions are given in (4.1) and (4.2), respectively. The wavevectors on the right-hand side of (4.1) and (4.2) may change along the

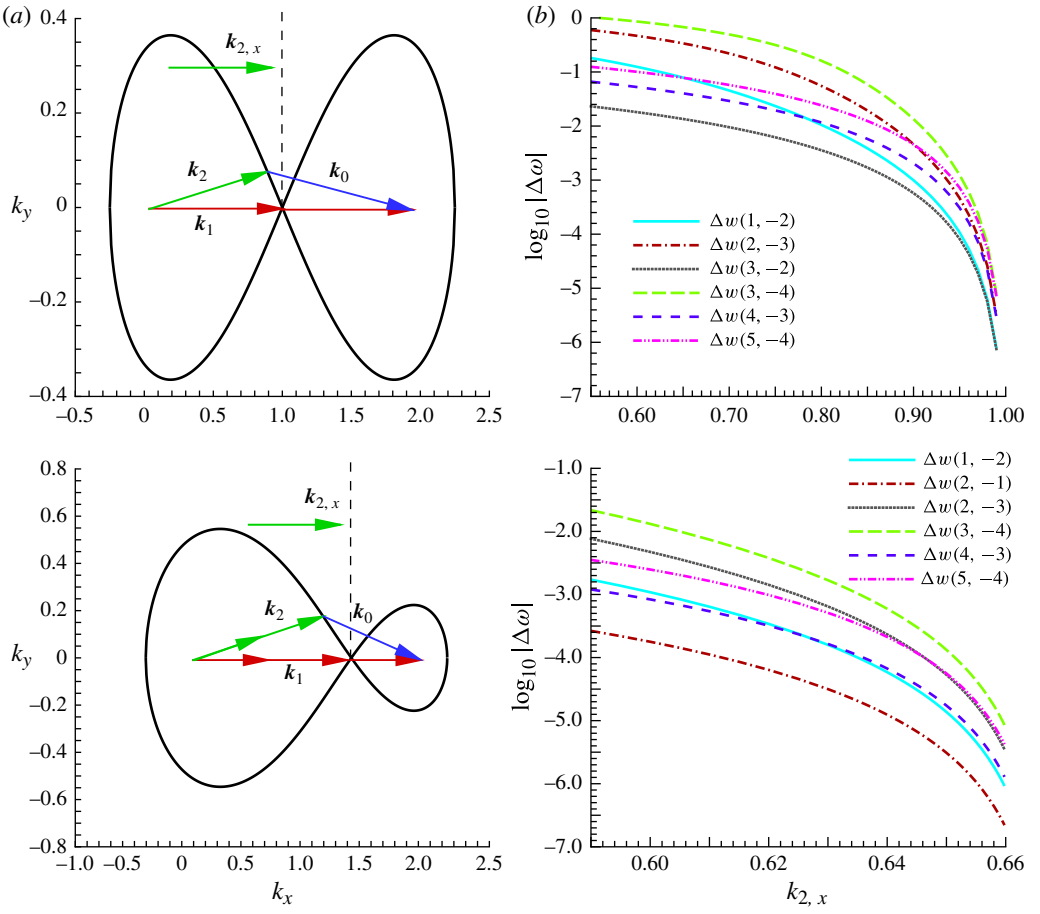

FIGURE 6. (Colour online) (*a*) Wavevector configuration and (*b*) frequency detuning of six near-resonant components: (top) quartet; (bottom) sextet.

corresponding linear resonance curves, as shown in the left-hand panels in figure 6. This process can be well defined through the x component of the wavevector of the second primary component $k_{2,x}$. In this section, we focus on the interval $0.55 < k_{2,x} < 1$ for a resonant quartet (case T1),

$$2\boldsymbol{k}_1 = \boldsymbol{k}_2 + \boldsymbol{k}_0, \quad 2|\boldsymbol{k}_1|^{1/2} = |\boldsymbol{k}_2|^{1/2} + |\boldsymbol{k}_0|^{1/2} = 2, \tag{4.1}$$

and $0.59 < k_{2,x} < 0.667$ for a resonant sextet (case T2),

$$3\boldsymbol{k}_1 = 2\boldsymbol{k}_2 + \boldsymbol{k}_0, \quad 3|\boldsymbol{k}_1|^{1/2} = 2|\boldsymbol{k}_2|^{1/2} + |\boldsymbol{k}_0|^{1/2} = \sqrt{6}. \tag{4.2}$$

In cases where the linear resonance condition is not exactly satisfied for the nearly resonant components, we introduce the frequency detuning

$$\Delta w(m, n) = \sqrt{|m\boldsymbol{k}_1 + n\boldsymbol{k}_2|} - \left|m\sqrt{|\boldsymbol{k}_1|} + n\sqrt{|\boldsymbol{k}_2|}\right| \tag{4.3}$$

to quantitatively identify them. Obviously, a small enough value of the frequency detuning $\Delta w(m, n)$ corresponds to a near-resonant wave component. It is found that

the frequency detuning of near-resonant components decrease rapidly as $k_{2,x}$ tends to 1 for a quartet, or to 0.667 for a sextet, respectively. For a quartet and sextet, the six near-resonant components with the smallest magnitude of the frequency detuning are shown in the right-hand panels in figure 6, respectively. Note that almost the same near-resonant components appear in both quartet and sextet, and they are all generated by $2N$-wave interactions, where $N = 2$, 3, 4 and even $N = 5$ is included. We define Π_e as the energy of the exact resonant set and Π_n as the energy of the six near-resonant components, respectively.

For the sake of computational efficiency, we first search for multiple solutions of initial approximations of the steady-state resonant waves by means of the HAM, and then use them as initial guess to obtain the convergent numerical results by means of the collocation method (see appendix B). In this way, we can quickly find the multiple steady-state resonant waves for complicated resonant wave systems, especially those with lots of near-resonant components studied in this section.

4.1. *Topology of a resonant quartet in parameter space*

Firstly, we investigate the topology of the energy distribution when the wavevectors change along the resonance curve in quartet (4.1). In a similar way as described in § 3, three groups of solutions are found in the case of $\varepsilon = 1.0001$, and the corresponding energy distributions are shown in figure 7. For all of the three groups, the energy distribution forms a continuum in the parameter space and changes dramatically as the x component of the second primary wavevector $k_{2,x}$ increases along the resonance curve (the corresponding wave patterns tend to long-crested waves), especially in the interval $k_{2,x} \in (0.9, 1)$.

When $k_{2,x} < 0.9$, very little wave energy is contained by the near-resonant components, thus the wave energy distribution is dominated by the exact resonance. When $0.9 < k_{2,x} < 1$, it is found that the wave energy distribution is dominated by both the exact and near-resonances, mainly because the magnitude of the frequency detuning of near-resonant components becomes so small (as shown in figure 6) that the near-resonances become important. As $k_{2,x}$ increases towards 1, the wave energy of the exact resonant component may either increase (figure 7*a*) or decrease (figure 7*b*,*c*), but the sum of the wave energy of the six near-resonant components always increases. Therefore, as $k_{2,x} \to 1$, i.e. wave patterns tend from two dimensions to one dimension, the interaction among different resonance sets may enhance or suppress the exact resonance, but always enhances the near-resonances as a whole. It is found that, when $k_{2,x} = 0.982$, the six near-resonant components together contain the majority of the total wave energy (46.11% in group 1, 82.65% in group 2 and 90.68% in group 3), which demonstrates the significance of the near-resonance in long-crested waves.

To further investigate the topology of the near-resonant components along the resonance curve, we consider the wave energy distribution in each near-resonant component, as shown in figure 8. Though the sum of the wave energy of the six near-resonant components always increases, the wave energy of each near-resonant component may either increase or decrease for all three groups of solutions. Thus, taking the exact resonance component into account, we conclude that the interaction between the exact resonance and near-resonances may either enhance or suppress each single resonant component.

Note that, in figure 8 at $k_{2,x} = 0.982$, the wave energy of the near-resonant components is mainly contained by the higher-order harmonics $\cos(3\xi_1 - 2\xi_2)$, $\cos(3\xi_1 - 4\xi_2)$, $\cos(4\xi_1 - 3\xi_2)$ and $\cos(5\xi_1 - 4\xi_2)$, which are generated by the six-wave,

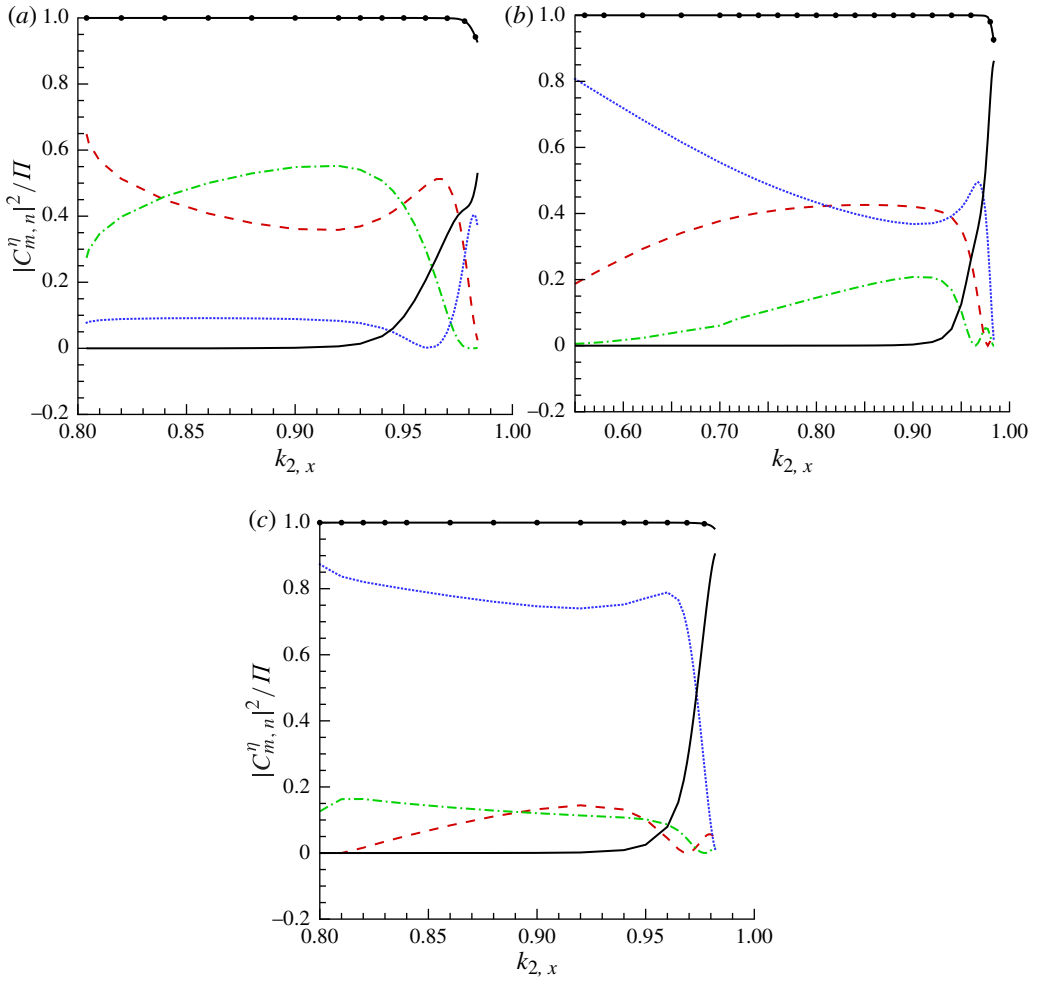

FIGURE 7. (Colour online) Wave energy distribution along the resonance curve in quartet (4.1) when $\varepsilon = 1.0001$: (*a*) group 1; (*b*) group 2; (*c*) group 3. Dashed line: $|C^{\eta}_{1,0}|^2/\Pi$ (first primary component). Dash-dotted line: $|C^{\eta}_{0,1}|^2/\Pi$ (second primary component). Dotted line: $|C^{\eta}_{2,-1}|^2/\Pi$ (exactly resonant component). Solid line: Π_n/Π (six near-resonant components). Solid line with circles: $(\Pi_e + \Pi_n)/\Pi$ (all the components considered).

eight-wave and even 10-wave interactions. These higher-order near-resonances do not disappear even as the wave patterns tend to long-crested ones. Moreover, the number of near-resonant wave components increases as the pattern tends towards one dimension. Note that similar phenomena have also been found by Ioualalen & Kharif (1993) and Badulin *et al.* (1995) for exact resonance on short-crested waves.

Secondly, we investigate the topology of wave energy distribution when wavevectors are given and ε (the ratio of the actual frequency to the linear frequency) increases. When $k_{2,x} = 0.9$, the wave energy distribution for all three groups of solutions in quartet (4.1) are shown in figure 9. Very little wave energy is contained by near-resonant components at $\varepsilon = 1.0001$. This can be found from figures 7 and 8, too. However, it is found that the near-resonant components as a whole contain more and

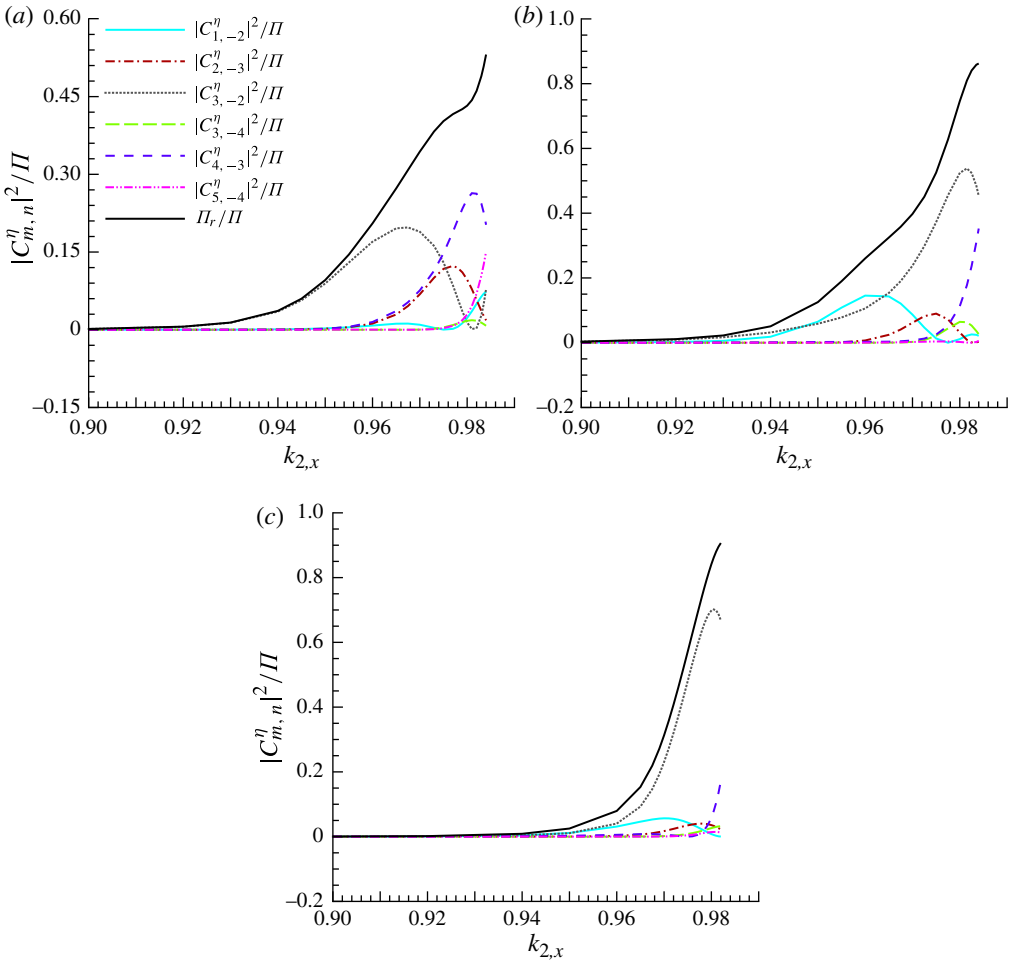

FIGURE 8. (Colour online) Wave energy distribution of six near-resonant components along the resonance curve in quartet (4.1) when $\varepsilon = 1.0001$: (*a*) group 1; (*b*) group 2; (*c*) group 3.

more wave energy as ε increases. Note that a larger value of ε often corresponds to larger wave amplitude, or higher nonlinearity. Thus, as the nonlinearity of a resonant quartet increases, all near-resonant waves as a whole contain more and more wave energy; the wave energy tends to transfer to the near-resonant components. This reveals the influence of nonlinearity on the wave energy distribution of resonant wave systems. Thus, for steady-state resonant waves with finite amplitudes, the near-resonance deserves more attention even than that of the exact resonance.

Thirdly, from a different viewpoint of the resulting continuum of patterns, we investigate the dependence of maximal instantaneous steepness on total wave energy. Here the maximal instantaneous steepness is defined as

$$H_{steepness} = \eta(\xi_1, \xi_2)_{\max}|\boldsymbol{k}_1|, \quad \text{for} \quad \xi_i \in [0, 2\pi]. \tag{4.4}$$

For $\boldsymbol{k}_2 = (0.90, 0.070227)$ and $1.0001 \leqslant \varepsilon \leqslant 1.002$, the maximal steepness in all of the three groups increases as the total energy increases, as shown in figure 10. As

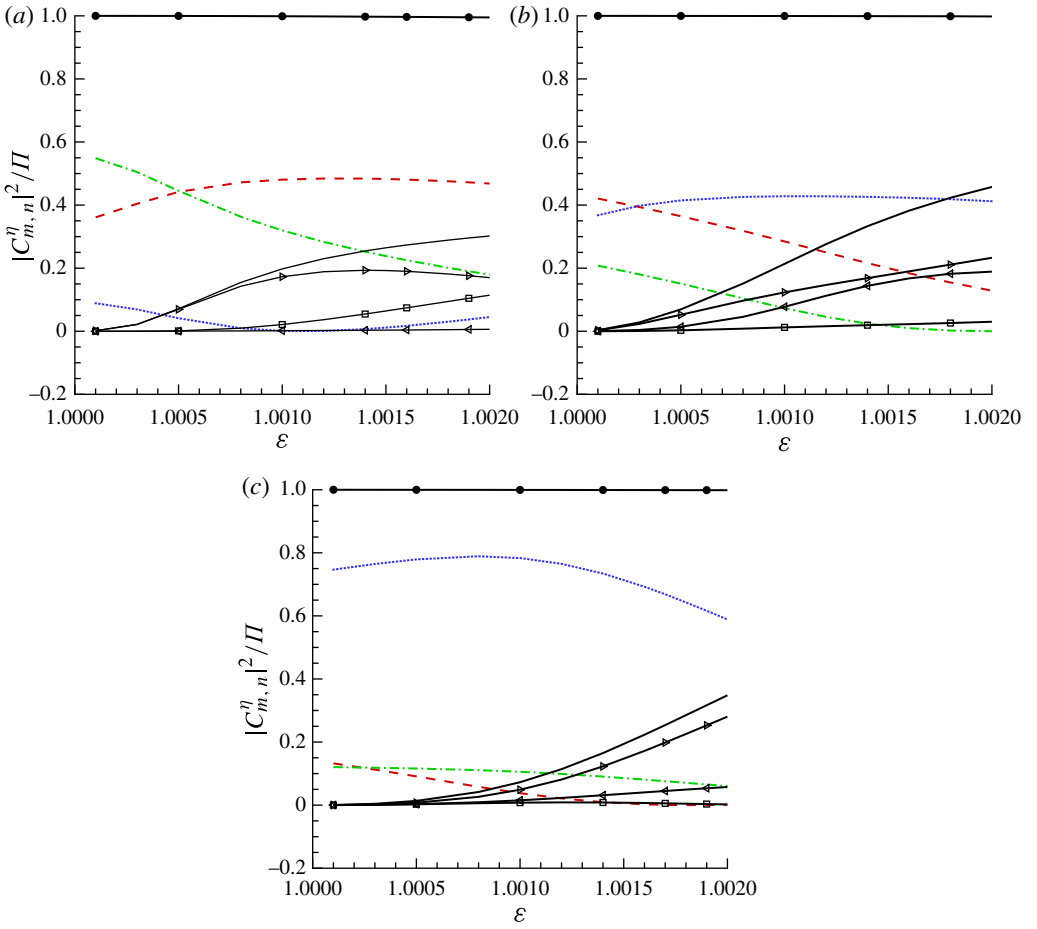

FIGURE 9. (Colour online) Wave energy distribution for increased dimensionless frequencies ε in quartet (4.1) when $\boldsymbol{k}_2 = (0.90, 0.070227)$: (*a*) group 1; (*b*) group 2; (*c*) group 3. Dashed line: $|C^{\eta}_{1,0}|^2/\Pi$ (first primary component). Dash-dotted line: $|C^{\eta}_{0,1}|^2/\Pi$ (second primary component). Dotted line: $|C^{\eta}_{2,-1}|^2/\Pi$ (exactly resonant component). Solid line: Π_n/Π (six near-resonant components). Solid line with left-pointing triangles: $|C^{\eta}_{1,-2}|^2/\Pi$. Solid line with right-pointing triangles: $|C^{\eta}_{3,-2}|^2/\Pi$. Solid line with squares: $|C^{\eta}_{4,-3}|^2/\Pi$. Solid line with circles: $(\Pi_e + \Pi_n)/\Pi$ (all components considered).

the maximal steepness increases, the state in group 3 tends to own more energy than that in the other two groups, as one component in group 3 owns the majority of the energy.

The surface elevations of the multiple steady-state resonant waves for quartet (4.1) in the case of $\boldsymbol{k}_2 = (0.90, 0.070227)$ and $\varepsilon = 1.001$ are as shown in figure 11. The perspective views of the three groups are in the left-hand column (see the corresponding supplementary movies available at http://dx.doi.org/10.1017/jfm.2014.2). Note that with angles close to the collinear limit, the wave pattern behaviour is like long-crested waves, which is warped by the wave group node. The elevations along the specific line $y = 0$ are shown in the right-hand column in figure 11. The large

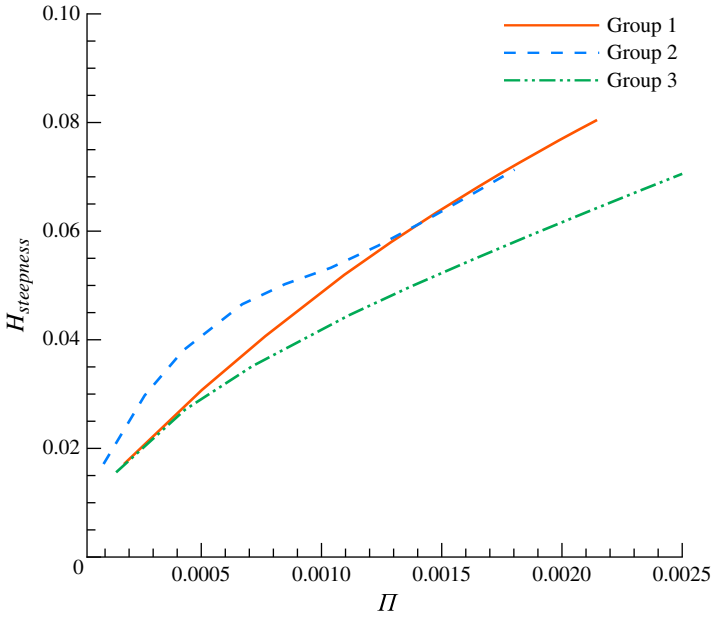

FIGURE 10. (Colour online) The dependence of maximal wave height on total wave energy for the three groups in quartet (4.1) when $\boldsymbol{k}_2 = (0.90, 0.070227)$ and $1.0001 \leqslant \varepsilon \leqslant 1.002$.

difference of elevation among the three groups demonstrates further the variety of energy distribution in a resonant set.

4.2. *Topology of a resonant sextet in parameter space*

The topology of wave energy distribution corresponding to a resonant sextet defined in (4.2) is plotted in figure 12. The left-hand column in figure 12 shows the energy distribution when the wavevectors change along the resonance curve of sextet (4.2) for $\varepsilon = 1.00001$. For the given wavevector $k_{2,x} = 0.625$ and the increased ε, the wave energy distribution is shown in the right-hand column of figure 12. For all three groups of steady-state resonant sextets, it is found that the near-resonant components as a whole contain more and more wave energy, when the wave patterns tend from two dimensions to one dimension, or when the nonlinearity of the resonant sextet increases. All this verifies the generality of our conclusions given in § 4.1. The dependence of maximal steepness on total wave energy for sextet (4.2) is given in figure 13. Note that, for a given total energy, the steady-state resonance wave in a sextet has a smaller maximal steepness compared with that in a quartet.

The close relation between resonance and bifurcation has long been observed: in some sense, they are similar phenomena, as regarded by Chen & Saffman (1978) and Roberts (1983). For steady-state resonance waves in sextet (4.2), a bifurcation caused by resonance is found, as shown in figure 14, which can be divided into three subregions, namely regions a, b and c, respectively. In region a, there exists only one steady-state resonant wave. Region b is dominated by the exact resonance, and region c is dominated by both the exact and near-resonances, as mentioned above. At the transition from region a to region b where the exact resonance becomes dominant,

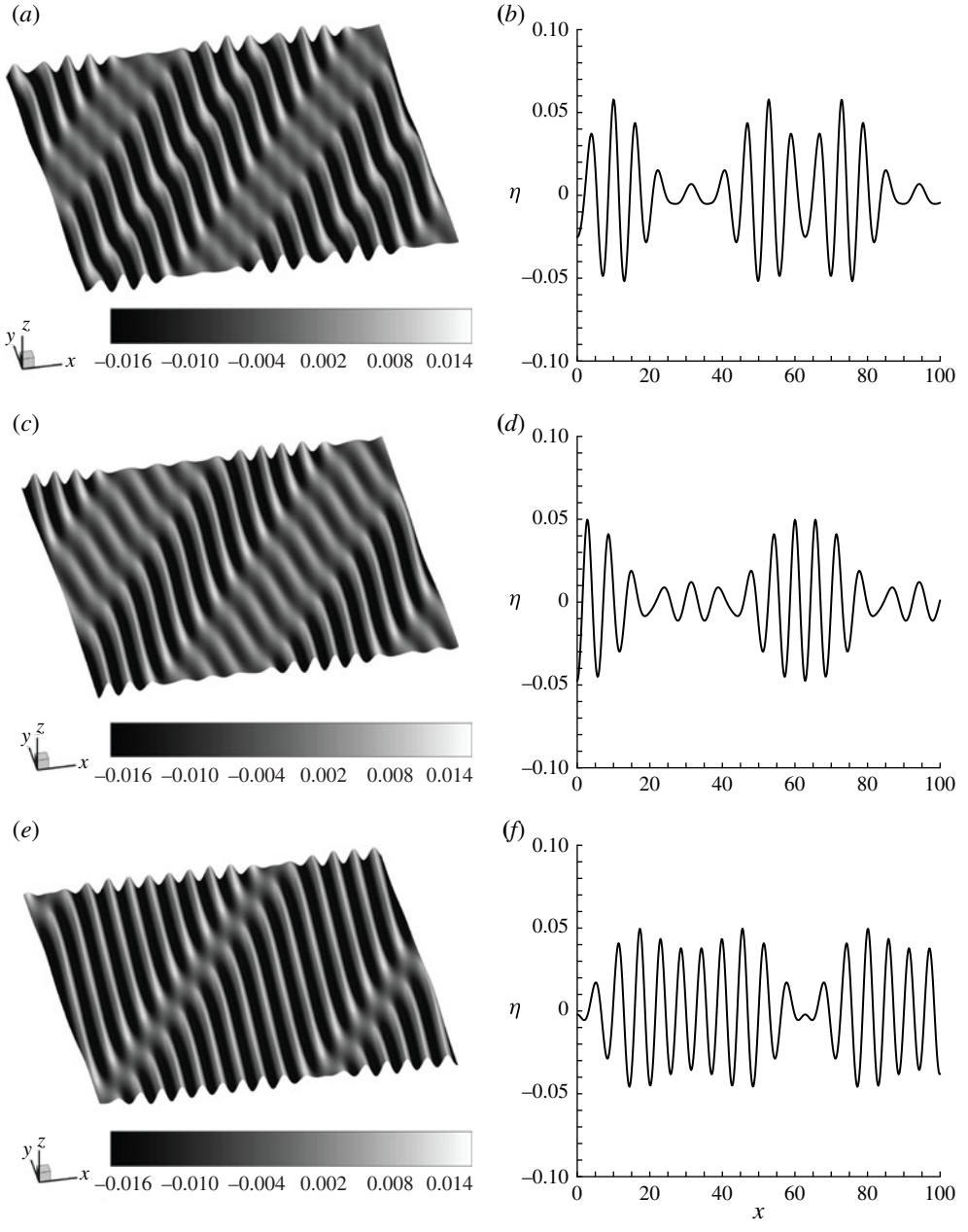

FIGURE 11. Surface elevation of the three groups in quartet (4.1) when $\boldsymbol{k}_2 = (0.90, 0.070227)$ and $\varepsilon = 1.001$: perspective views in (*a*) group 1, (*c*) group 2 and (*e*) group 3; and elevation along line $y = 0$ in (*b*) group 1, (*d*) group 2 and (*f*) group 3.

the original trivial solution bifurcates into two steady-state resonant waves. It seems that more steady-state resonant waves should exist in region c, since a series of near-resonances are excited at the transition from region b to region c.

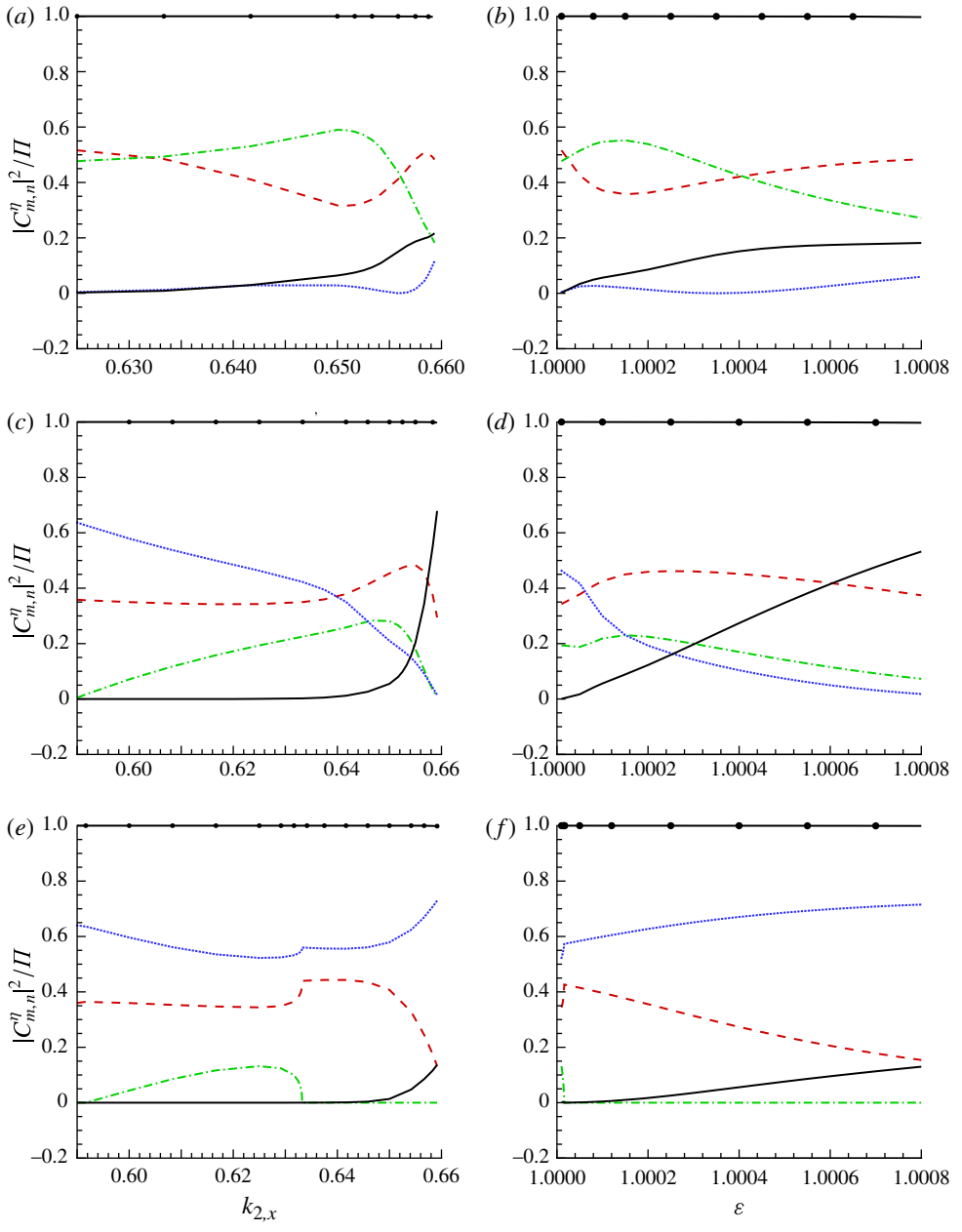

FIGURE 12. (Colour online) Wave energy distribution in sextet (4.2): $\varepsilon = 1.00001$ as wavevectors changed along the resonance curve in (*a*) group 1, (*c*) group 2 and (*e*) group 3; and $k_{2,x} = 0.625$ as dimensionless frequencies ε increased in (*b*) group 1, (*d*) group 2 and (*f*) group 3. Dashed line: $|C^{\eta}_{1,0}|^2/\Pi$ (first primary component). Dash-dotted line: $|C^{\eta}_{0,1}|^2/\Pi$ (second primary component). Dotted line: $|C^{\eta}_{3,-2}|^2/\Pi$ (exactly resonant component). Solid line: Π_n/Π (six near-resonant components). Solid line with circles: $(\Pi_e + \Pi_n)/\Pi$ (all components considered).

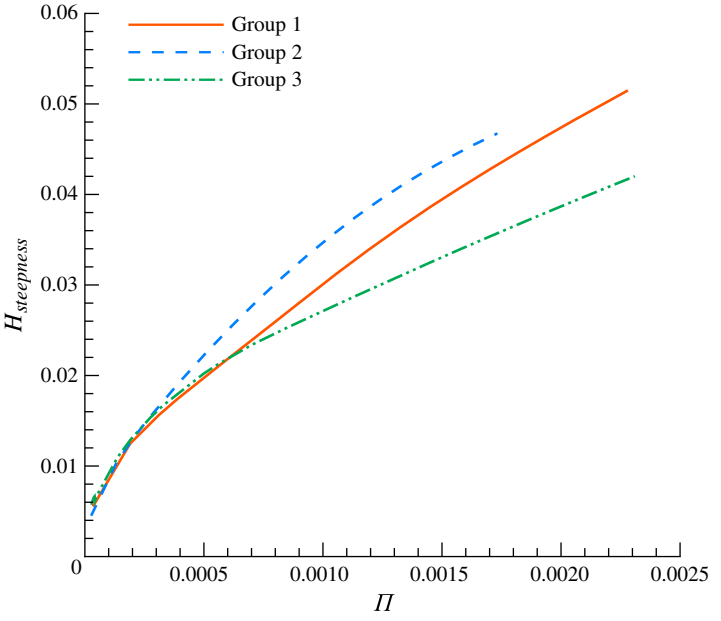

FIGURE 13. (Colour online) The dependence of maximal wave height on total wave energy for the three groups in sextet (4.2) when $k_{2,x} = 0.625$ and $1.00001 \leqslant \varepsilon \leqslant 1.0008$.

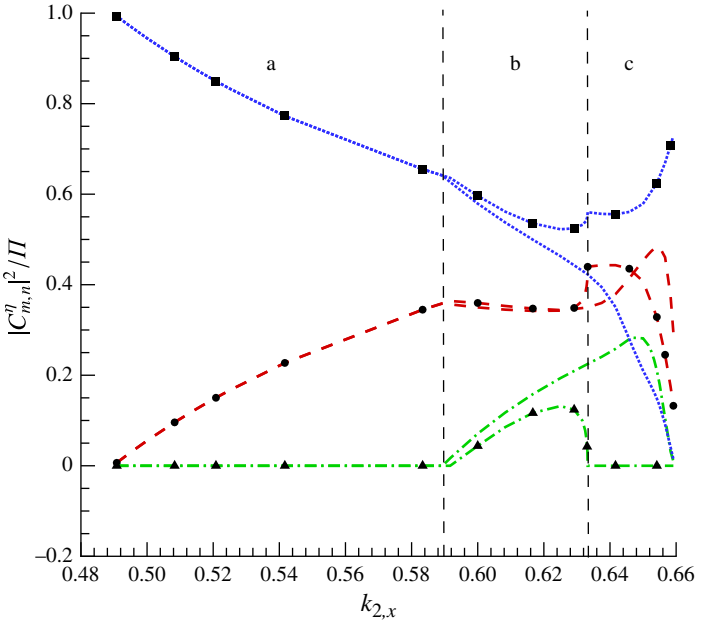

FIGURE 14. (Colour online) Bifurcation due to resonant interactions in sextet (4.2) when $\sigma_i/w_i = 1.00001$: lines without points, group 2; lines with points, group 3.

5. Stability analysis

In this section, we consider the linear stability of the steady-state resonant waves in deep water to an infinitesimal disturbance.

5.1. *Mathematical derivation*

For simplicity, we take the steady-state resonance quartet (4.1) as the unperturbed wave. Let

$$\eta(\xi_1, \xi_2, t) = \bar{\eta}(\xi_1, \xi_2) + \eta'(\xi_1, \xi_2, t), \tag{5.1}$$

$$\phi(\xi_1, \xi_2, z, t) = \bar{\phi}(\xi_1, \xi_2, z) + \phi'(\xi_1, \xi_2, z, t), \tag{5.2}$$

where $(\bar{\eta}, \bar{\phi})$ and (η', ϕ') denote, respectively, the unperturbed and infinitesimal perturbative motions $(\eta' \ll \bar{\eta},\ \phi' \ll \bar{\phi})$.

Substituting (5.1) and (5.2) into the original equations (2.1)–(2.4) and recasting them in the coordinate system (ξ_1, ξ_2, z, t), we obtain the first-order perturbation equations

$$\nabla^2\phi' = 0, \quad z \leqslant \bar{\eta}(\xi_1, \xi_2), \tag{5.3}$$

$$\left.\begin{aligned} \phi'_t + R_1\phi'_{\xi_1} + R_2\phi'_{\xi_2} + \bar{\phi}_z\phi'_z + R_3\eta' = 0, \\ \eta'_t + R_4\eta' + R_1\eta'_{\xi_1} + R_2\eta'_{\xi_2} + R_5\phi'_{\xi_1} + R_6\phi'_{\xi_2} - \phi'_z = 0, \end{aligned}\right\} \quad z = \bar{\eta}(\xi_1, \xi_2), \tag{5.4}$$

$$\frac{\partial\phi'}{\partial z} = 0, \quad \text{as} \quad z \to -\infty, \tag{5.5}$$

where

$$R_1 = -\sigma_1 + k_1^2\bar{\phi}_{\xi_1} + \boldsymbol{k}_1 \cdot \boldsymbol{k}_2\bar{\phi}_{\xi_2}, \tag{5.6}$$

$$R_2 = -\sigma_2 + k_2^2\bar{\phi}_{\xi_2} + \boldsymbol{k}_1 \cdot \boldsymbol{k}_2\bar{\phi}_{\xi_1}, \tag{5.7}$$

$$R_3 = g - \sigma_1\bar{\phi}_{\xi_1,z} - \sigma_2\bar{\phi}_{\xi_2,z} + k_1^2\bar{\phi}_{\xi_1}\bar{\phi}_{\xi_1,z} + k_2^2\bar{\phi}_{\xi_2}\bar{\phi}_{\xi_2,z} + \boldsymbol{k}_1 \cdot \boldsymbol{k}_2(\bar{\phi}_{\xi_1,z}\bar{\phi}_{\xi_2} + \bar{\phi}_{\xi_1}\bar{\phi}_{\xi_2,z}) + \bar{\phi}_z\bar{\phi}_{zz}, \tag{5.8}$$

$$R_4 = k_1^2\bar{\phi}_{\xi_1,z}\bar{\eta}_{\xi_1} + k_2^2\bar{\phi}_{\xi_2,z}\bar{\eta}_{\xi_2} + \boldsymbol{k}_1 \cdot \boldsymbol{k}_2\left(\bar{\phi}_{\xi_1,z}\bar{\eta}_{\xi_2} + \bar{\phi}_{\xi_2,z}\bar{\eta}_{\xi_1}\right) - \bar{\phi}_{zz}, \tag{5.9}$$

$$R_5 = k_1^2\bar{\eta}_{\xi_1} + \boldsymbol{k}_1 \cdot \boldsymbol{k}_2\bar{\eta}_{\xi_2}, \tag{5.10}$$

$$R_6 = k_2^2\bar{\eta}_{\xi_2} + \boldsymbol{k}_1 \cdot \boldsymbol{k}_2\bar{\eta}_{\xi_1}, \tag{5.11}$$

and $k_i = |\boldsymbol{k}_i|$. We look for non-trivial solutions of (5.4) of the form

$$\eta' = \mathrm{e}^{-\mathrm{i}\sigma t}\mathrm{e}^{\mathrm{i}(p'\xi_1 + q'\xi_2)} \sum_{J=-\infty}^{\infty}\sum_{K=-\infty}^{\infty} a_{JK}\mathrm{e}^{\mathrm{i}(J\xi_1 + K\xi_2)}, \tag{5.12}$$

$$\phi' = \mathrm{e}^{-\mathrm{i}\sigma t}\mathrm{e}^{\mathrm{i}(p'\xi_1 + q'\xi_2)} \sum_{J=-\infty}^{\infty}\sum_{K=-\infty}^{\infty} b_{JK}\mathrm{e}^{\mathrm{i}(J\xi_1 + K\xi_2)}\mathrm{e}^{\kappa_{JK}z}, \tag{5.13}$$

where $\kappa_{JK} = \{[(p' + J)k_{1,x} + (q' + K)k_{2,x}]^2 + [(p' + J)k_{1,y} + (q' + K)k_{2,y}]^2\}^{1/2}$, and (p', q') is the wavevector of perturbation for the linear case in the new coordinate system (ξ_1, ξ_2, z, t). The corresponding wavevector in the Cartesian coordinate system is $(k_p, k_q) = (p'k_{1,x} + q'k_{2,x},\ p'k_{1,y} + q'k_{2,y})$. The coefficients a_{JK}, b_{JK} and the eigenvalue σ, the frequency of the perturbations, can be determined once the unperturbed waves

$\bar{\eta}$ and $\bar{\phi}$ are known. Instability corresponds to $\mathrm{Im}(\sigma) \neq 0$ as eigenvalues σ appear in complex conjugate pairs.

When no unperturbed wave exist in the wave field, $\bar{\eta} = \bar{\phi} = 0$ with $\sigma_i = \sqrt{g|\boldsymbol{k}_i|}$. Then the eigenvalues are

$$\sigma_{JK}^{s} = \sqrt{g}\{-[|\boldsymbol{k}_1|^{1/2}(p' + J) + |\boldsymbol{k}_2|^{1/2}(q' + K)] + s\kappa_{JK}^{1/2}\}, \quad s = \pm 1. \tag{5.14}$$

The sign of s defines the direction of propagation of the disturbance in the (ξ_1, ξ_2, z, t) coordinate system. Note that the degeneracy with respect to p' and q',

$$\sigma_{JK}^{s}(p', q') = \sigma_{J-M,K-N}^{s}(p' + M, q' + N), \quad (M, N) \in N^2, \tag{5.15}$$

also appears as in the work of McLean (1982) and Ioualalen & Kharif (1994).

Once unperturbed wave appears in the wave field, instabilities can arise if the eigenvalues satisfy

$$\sigma_{J_1K_1}^{s_1}(p', q') = \sigma_{J_2K_2}^{s_2}(p', q'). \tag{5.16}$$

This corresponds to the necessary condition formulated by MacKay & Saffman (1986) that the unperturbed wave can lose spectral stability with finite-amplitude effects if two simple eigenvalues coalesce with opposite signature or at zero frequency. A similar criterion has also been obtained by Badulin *et al.* (1995), who proposed an asymptotic procedure on the instability of short-crested water waves.

In a linear approximation the condition when instability happens may be reduced to

$$\kappa_{J_1K_1}^{1/2} + \kappa_{J_2K_2}^{1/2} = (J_1 - J_2)|\boldsymbol{k}_1|^{1/2} + (K_1 - K_2)|\boldsymbol{k}_2|^{1/2}, \tag{5.17}$$

with $s_1 = -s_2 = 1$. Alternatively, the above criterion may be written as

$$\begin{aligned}&[(k_p + k_{J_1K_1,x})^2 + (k_q + k_{J_1K_1,y})^2]^{1/4} + [(k_p + k_{J_2K_2,x})^2 + (k_q + k_{J_2K_2,y})^2]^{1/4} \\ &\quad = \tilde{\omega}_{J_1K_1} - \tilde{\omega}_{J_2K_2},\end{aligned} \tag{5.18}$$

where $\boldsymbol{k}_{JK} = (Jk_{1,x} + Kk_{2,x}, \quad Jk_{1,y} + Kk_{2,y})$ and $\tilde{\omega}_{JK} = J|\boldsymbol{k}_1|^{1/2} + K|\boldsymbol{k}_2|^{1/2}$ are the corresponding wavenumber and frequency depending on J and K. Following McLean (1982) and Ioualalen & Kharif (1994), we define two general classes of instabilities from (5.18): class I corresponds to $J_1 + K_1 - J_2 - K_2$ even, and class II corresponds to $J_1 + K_1 - J_2 - K_2$ odd. Considering the degeneracy noted above, we may further choose J_i and K_i so that

$$\left.\begin{array}{lll} J_1 + K_1 = j, & J_2 + K_2 = -j & \text{for the class I}(j), \\ J_1 + K_1 = j, & J_2 + K_2 = -j - 1 & \text{for the class II}(j), \end{array}\right\} \quad j = 1, 2, 3, \ldots. \tag{5.19}$$

For a weakly nonlinear unperturbed wave, like the small-amplitude steady-state resonance waves, the instability caused by higher-order resonances are very weak (Zakharov 1968). Thus we focus on the class I for $j = 1$, which corresponds to the dominant instability caused by four-wave interactions. For simplicity, $\varepsilon = 1.0001$ and $k_{2,x} = 0.9$ in (4.1) are applied so that only the two primary components together with the exact resonant one are non-trivial in the basic wave.

Given the symmetry in the basic wave, we consider the following five cases, which belong to classes Ia and Ib, respectively:

$$\text{Ia:} \quad \begin{cases} J_1 = 0, & K_1 = 1, & J_2 = -1, & K_2 = 0, \\ J_1 = 1, & K_1 = 0, & J_2 = -2, & K_2 = 1, \end{cases} \tag{5.20}$$

$$\text{Ib:}\ \begin{cases} J_1 = 0, & K_1 = 1, & J_2 = 0, & K_2 = -1, \\ J_1 = 1, & K_1 = 0, & J_2 = -1, & K_2 = 0, \\ J_1 = 2, & K_1 = -1, & J_2 = -2, & K_2 = 1. \end{cases} \tag{5.21}$$

The coalescence of the eigenvalues can alternatively be interpreted as a resonance of two infinitesimal modes of wavevectors $\boldsymbol{k}_1'$ and $\boldsymbol{k}_2'$ with the fundamental components of wavevectors $\bar{\boldsymbol{k}}_1$ and $\bar{\boldsymbol{k}}_2$ in the basic wave. In the Cartesian coordinate system, the resonance condition

$$\boldsymbol{k}_1' + \boldsymbol{k}_2' = \bar{\boldsymbol{k}}_1 + \bar{\boldsymbol{k}}_2, \quad \omega_1' + \omega_2' = \bar{\omega}_1 + \bar{\omega}_2, \tag{5.22}$$

is satisfied, where ω_i' and $\bar{\omega}_i$ denote the frequencies of the corresponding perturbed and unperturbed waves, respectively. For example, the first case in (5.20) corresponds to

$$\boldsymbol{k}_1' = (k_p + k_{2,x},\ \ k_q + k_{2,y})^t, \quad \boldsymbol{k}_2' = (k_p - k_{1,x},\ \ k_q - k_{1,y})^t, \tag{5.23}$$

$$\bar{\boldsymbol{k}}_1 = \boldsymbol{k}_2, \quad \bar{\boldsymbol{k}}_2 = \boldsymbol{k}_1, \tag{5.24}$$

$$\omega_1' = |\boldsymbol{k}_1'|^{1/2} = [(k_p + k_{2,x})^2 + (k_q + k_{2,y})^2]^{1/4}, \tag{5.25}$$

$$\omega_1' = |\boldsymbol{k}_2'|^{1/2} = [(k_p - k_{1,x})^2 + (k_q - k_{1,y})^2]^{1/4}, \tag{5.26}$$

$$\bar{\omega}_1 = |\bar{\boldsymbol{k}}_1|^{1/2} = |\boldsymbol{k}_2|^{1/2}, \quad \bar{\omega}_2 = |\bar{\boldsymbol{k}}_2|^{1/2} = |\boldsymbol{k}_1|^{1/2}, \tag{5.27}$$

in (5.22). Once the values of J and K are given, the resonance condition (5.18) is determined; the five cases defined in (5.20) and (5.21) are plotted in figure 15. As more components in the basic wave need to be considered, compared with that of the Stokes wave (McLean 1982) and short-crested waves (Ioualalen & Kharif 1994), the instability region predicted by the linear resonance condition (5.18) should be wider than that of the former works.

5.2. *Numerical approach*

The expressions in (5.12) and (5.13) are truncated with J and K up to N, and substituted into (5.4). Then, we obtain the following eigenvalue problem for σ with eigenvector $\boldsymbol{u} = (a_{JK}, b_{JK})^t$:

$$\boldsymbol{A}\boldsymbol{u} = \mathrm{i}\sigma \boldsymbol{B}\boldsymbol{u}. \tag{5.28}$$

Matrices $\boldsymbol{A}$ and $\boldsymbol{B}$ are complex ones that depend on the basic wave and the wavenumbers k_p and k_q (p' and q'). The detailed expressions for $\boldsymbol{A}$ and $\boldsymbol{B}$ are given in appendix C.

Ioualalen & Kharif (1994) compared the computational efficiencies of the collocation method and the Galerkin method. They found that both methods are of the same order of accuracy for small wave steepness. In this work, the collocation method is applied by enforcing (5.28) to be satisfied at $(2N+1)(2N+1)$ points distributed over one period of the free surface in the two horizontal directions ξ_1 and ξ_2.

The small nonlinear effects of unperturbed wave are expected to produce bands of instability in the neighbourhood of the loci of collisions of the eigenvalues (Francius & Kharif 2006), so the linear resonance curves shown in figure 15 may be a reasonable prediction of where instability happens as the amplitudes of the components in the basic wave (4.1) are quite small, $a_i k_i < 0.01$. For steady-state resonance waves, our numerical results confirm that instability does happen along the linear resonance

	$k_q = 0.3176$		$k_q = -0.3176$	
N	Im(σ)	Re(σ)	Im(σ)	Re(σ)
13	0.210616(−03)	−0.338311(−02)	0.532218(−04)	1.48349
15	0.222869(−03)	−0.349616(−02)	0.531804(−04)	1.48349
17	0.219439(−03)	−0.348663(−02)	0.531800(−04)	1.48349
19	0.222381(−03)	−0.349546(−02)	0.531806(−04)	1.48349
21	0.222380(−03)	−0.349546(−02)	0.531806(−04)	1.48349
23	0.222381(−03)	−0.349546(−02)	0.531806(−04)	1.48349

TABLE 10. Examples of the dependence of the eigenvalues on the truncation. Specification: $\boldsymbol{k}_2 = (0.9, 0.070227)$ in quartet (4.1), $\varepsilon = 1.0001$ and $k_p = 0.55$.

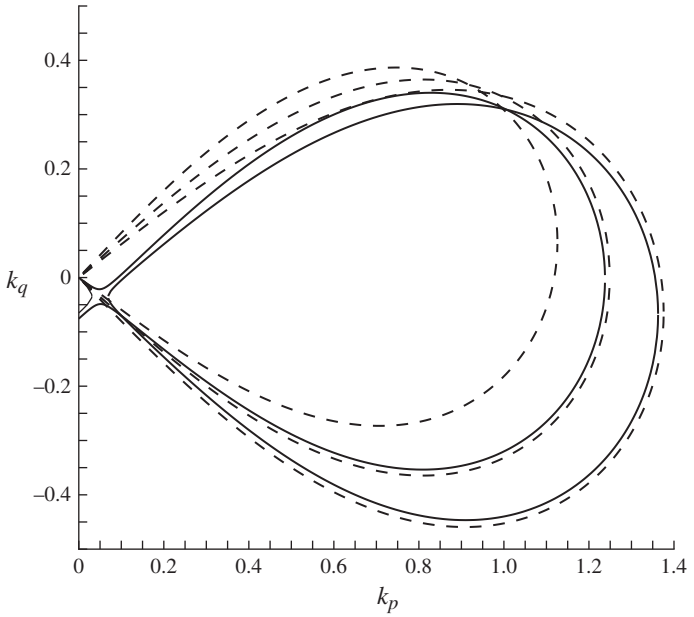

FIGURE 15. Resonance curves of classes Ia and Ib from the linear dispersion relation when $k_{2,x} = 0.9$ in (4.1): solid line, class Ia; dashed line, class Ib.

curves. For example, the eigenvalues of two points in the (k_p, k_q) plane that laid on the resonance curves are shown in table 10, where the dependence of the eigenvalues on the truncation is also given.

Note that the two points in table 10 are symmetrical about the line $k_q = 0$, whereas their eigenvalues converge to different values. This lack of symmetry is due to the interaction of instabilities (Badulin *et al.* 1995), as all the resonance curves overlap each other in the whole region and two of them are asymmetrical about the line $k_q = 0$.

In summary, according to our calculations, the steady-state resonant waves are stable as long as the disturbance does not resonate with any components of the basic wave. This conclusion qualitatively agrees with that for the Stokes waves and short-crested waves, and thus is reasonable. The interaction between instabilities is not the primary objective of the present work, and the instability region of steady-state

resonance waves will be the object of a further paper for more noticeable wave patterns.

6. Conclusion and discussion

In this paper, we investigate steady-state resonance of multiple wave interactions in deep water. The fully nonlinear wave equations are solved for both exact and near-resonances. Here, both Phillips' linear resonance conditions (1.1) together with the nonlinear ones (1.2) based on the actual frequency are satisfied simultaneously by exact resonance sets.

Firstly, unlike Liao (2011) and Xu *et al.* (2012), who considered only a special resonant quartet corresponding to $C = 2$ in (3.2), we investigated the existence of steady-state resonant waves in more general and complicated cases, including general resonant quartets for arbitrary C in (3.2), three coupled resonant quartets, and even a resonant sextet. It is found that the multiple steady-state resonant waves exist in all considered cases. Besides, the number of multiple solutions tends to increase as more wave components are involved in the resonant sets. All of these verify that multiple steady-state resonant waves indeed exist widely in general.

Secondly, we studied the topology of steady-state resonant waves in parameter space, and revealed the significant role of the near-resonance. It is found that all of the near-resonant components as a whole contain more and more wave energy, as resonant wave patterns tend from two dimensions to one dimension, or as the nonlinearity of the resonant wave system increases. The maximal instantaneous steepness increases as the total energy increases and it has a larger value in a quartet than that in a sextet. Besides, a bifurcation of steady-state resonant waves due to resonance is found in a sextet.

Finally, we analysed the linear stability of the steady-state resonant waves. Based on the numerical procedure applied by McLean (1982) and Ioualalen & Kharif (1994), we developed it further to investigate the stability of steady-state resonant waves to infinitesimal three-dimensional perturbations of arbitrary wavelength. It is found that the steady-state resonant waves are stable as long as the disturbance does not resonate with any components of the basic wave. Here the stability is with respect to perturbations belonging to the same specific manifold in the wavenumber space as the steady-state resonant waves. Considering the infinitesimal amplitude of perturbations, there might be a considerable time lag until the generic perturbations become important and destabilize the steady-state wave pattern. Thus the steady-state resonance waves will be, at least in principle, metastable three-dimensional waves, which might be observed in experiments.

To the best of our knowledge, the above-mentioned results have never been reported for the steady-state resonant wave systems. All of them are helpful to enrich and deepen our understanding about resonant gravity waves.

In this article, the homotopy analysis method (HAM) is successfully applied to gain the multiple steady-state resonant waves. To verify the multiple steady-state resonant waves found by the HAM, the collocation method (see appendix B) is applied using initial approximations found by the HAM as a starting point of iteration. It is found that both the analytic and numerical methods converge to the same results. This confirms the correctness of our solutions. For the sake of computational efficiency, this combined approach is used to study the topology of steady-state resonant waves in parameter space and to analyse the stability of the steady-state resonant waves.

As mentioned in the introduction, for the sake of simplicity, we assume that the ratio of the actual frequency to the corresponding linear ones of each exact resonant

component is the same. In this case, both Phillips' linear resonance condition together with the nonlinear ones are satisfied at the same time. However, it is worth mentioning that the existence of multiple steady-state resonance waves depends only upon the nonlinear resonance condition, and it is not necessary to satisfy Phillips' linear resonance condition in general cases. When the nonlinear resonance condition is satisfied, but the frequency ratio of each exact resonant component is not the same, Phillips' linear resonance condition is no longer satisfied. However, even in this general case, the convergent analytic approximations of multiple resonant waves have been obtained by means of the HAM using such a new linear operator,

$$\mathcal{L}^p[\phi] = \sum_{i=1}^{\kappa}\sum_{j=1}^{\kappa}\sigma_i\sigma_j\frac{\partial^2\phi}{\partial\xi_i\partial\xi_j} + \varepsilon^2 g\frac{\partial\phi}{\partial z}, \tag{6.1}$$

where

$$\varepsilon = \begin{cases} \varepsilon_1, & m_1 = 1,\ m_2 = 0,\ \ldots,\ m_\kappa = 0, \\ \varepsilon_2, & m_1 = 0,\ m_2 = 1,\ \ldots,\ m_\kappa = 0, \\ \vdots & \vdots \\ \varepsilon_\kappa, & m_1 = 0,\ m_2 = 0,\ \ldots,\ m_\kappa = 1, \\ \varepsilon_{0,1}, & m_i = m_{1,i}, \\ \varepsilon_{0,2}, & m_i = m_{2,i}, \\ \vdots & \vdots \\ \varepsilon_{0,l}, & m_i = m_{l,i}, \\ 1, & \text{else}. \end{cases} \tag{6.2}$$

is a piecewise parameter whose value depends on the subscript m_i in ϕ expressed by (2.12) and (2.13), ε_i denotes the frequency ratio of the ith primary component, and $\varepsilon_{0,i}$ is the frequency ratio of the ith resonant component, respectively. Here, we consider l resonant wave components generated by κ primary wave components. The homogeneous solutions of this piecewise linear operator (6.1) satisfy all of the l nonlinear resonance conditions

$$\begin{cases} m_{\iota,1}\boldsymbol{k}_1 + m_{\iota,2}\boldsymbol{k}_2 + \cdots + m_{\iota,\kappa}\boldsymbol{k}_\kappa + \boldsymbol{k}_{0,\iota} = 0, \\ m_{\iota,1}\sigma_1 + m_{\iota,2}\sigma_2 + \cdots + m_{\iota,\kappa}\sigma_\kappa + \sigma_{0,\iota} = 0, \end{cases} \quad \iota = 1, 2, \ldots, l. \tag{6.3}$$

Considering the limited length of this paper, we neglect the details of the mathematics, and just mention that convergent analytic approximations of multiple steady-state resonant waves based on this kind of piecewise linear operator are obtained, which will be reported in future. This is mainly because the HAM provides great freedom to choose such a proper auxiliary linear operator, as pointed out by Liao (2012).

Obviously, it is important to reproduce the steady-state resonant waves in experiments. Besides, for the L_1–L_4 'horseshoe' patterns (Fructus *et al.* 2005) caused by a resonant quintet, we have not found steady-state resonant waves. This is not surprising, since steady-state resonant waves do not absolutely exist in arbitrary cases, as pointed out by Xu *et al.* (2012). Note that Shrira, Badulin & Kharif (1996) qualitatively analysed the persistent character of 'horseshoe' patterns by taking the pumping and dissipation into consideration. So, generalizing the existing procedure to cover non-conservative effects may be a promising attempt for a quintet. All of these issues are interesting and deserve further investigations in future.

Acknowledgements

We would like to express our sincere thanks to Prof. Roger Grimshaw, Prof. Per A. Madsen, Prof. Christian Kharif and Dr Yuming Liu for their helpful and enlightening discussions. Thanks also go to the anonymous reviewers for their valuable comments and suggestions, which greatly enhanced the quality of this article. We are grateful to the National Natural Science Foundation (Approval No. 11272209) and State Key Laboratory of Ocean Engineering (Approval No. GKZD010059) for financial support. This work is also partly supported by the Lloyd's Register Foundation (LRF). Lloyd's Register Foundation helps to protect life and property by supporting engineering-related education, public engagement and the application of research.

Supplementary movies

Supplementary movies are available at http://dx.doi.org/10.1017/jfm.2014.2.

Appendix A. Solution procedure of the homotopy analysis method

First, we construct a family of partial differential equations (PDEs) about two homotopies $\breve{\phi}(\xi_1, \xi_2, \ldots, \xi_\kappa, z; q)$ and $\breve{\eta}(\xi_1, \xi_2, \ldots, \xi_\kappa; q)$, governed by the so-called zeroth-order deformation equations,

$$(1-q)\mathcal{L}[\breve{\phi}(\xi_1, \xi_2, \ldots, \xi_\kappa, z; q) - \phi_0(\xi_1, \xi_2, \ldots, \xi_\kappa, z)] = qc_0\mathcal{N}_1[\breve{\phi}(\xi_1, \xi_2, \ldots, \xi_\kappa, z; q)], \tag{A 1}$$

$$(1-q)\breve{\eta}(\xi_1, \xi_2, \ldots, \xi_\kappa; q) = qc_0\mathcal{N}_2[\breve{\eta}(\xi_1, \xi_2, \ldots, \xi_\kappa; q), \breve{\phi}(\xi_1, \xi_2, \ldots, \xi_\kappa, z; q)], \tag{A 2}$$

where $q \in [0, 1]$ denotes an embedding parameter, $c_0 \neq 0$ is the so-called convergence-control parameter, $\mathcal{L}$ is an auxiliary linear operator, and $\mathcal{N}_1$ and $\mathcal{N}_2$ are nonlinear operators defined in (2.7) and (2.8), respectively.

Assuming that the convergence-control parameter c_0 is properly chosen so that the Maclaurin series of $\breve{\phi}(\xi_1, \xi_2, \ldots, \xi_\kappa, z; q)$ and $\breve{\eta}(\xi_1, \xi_2, \ldots, \xi_\kappa; q)$, with respect to the embedding parameter q,

$$\breve{\phi}(\xi_1, \xi_2, \ldots, \xi_\kappa, z; q) = \sum_{m=0}^{+\infty} \phi_m(\xi_1, \xi_2, \ldots, \xi_\kappa, z)q^m, \tag{A 3}$$

$$\breve{\eta}(\xi_1, \xi_2, \ldots, \xi_\kappa; q) = \sum_{m=0}^{+\infty} \eta_m(\xi_1, \xi_2, \ldots, \xi_\kappa)q^m, \tag{A 4}$$

exist and converge at $q = 1$, we have the so-called homotopy-series solution

$$\phi(\xi_1, \xi_2, \ldots, \xi_\kappa, z) = \sum_{m=0}^{+\infty} \phi_m(\xi_1, \xi_2, \ldots, \xi_\kappa, z), \tag{A 5}$$

$$\eta(\xi_1, \xi_2, \ldots, \xi_\kappa) = \sum_{m=0}^{+\infty} \eta_m(\xi_1, \xi_2, \ldots, \xi_\kappa), \tag{A 6}$$

respectively. The unknown term $\phi_m(\xi_1, \xi_2, \ldots, \xi_\kappa, z)$ is governed by a linear PDE and $\eta_m(\xi_1, \xi_2, \ldots, \xi_\kappa)$ is straightforward to obtain.

Based on the freedom in the choice of auxiliary linear operator and the linear part of (2.7), we define

$$\mathcal{L}[\phi]=\sum_{i=1}^{\kappa}\sum_{j=1}^{\kappa}\omega_i\omega_j\frac{\partial^2\phi}{\partial\xi_i\partial\xi_j}+g\frac{\partial\phi}{\partial z}, \tag{A 7}$$

where

$$\omega_i=\sqrt{g|\boldsymbol{k}_i|},\quad i=1,2,\ldots,\kappa \tag{A 8}$$

is the linear frequency of the ith primary wave.

Substituting the Maclaurin series (A 3)–(A 4) into the zeroth-order deformation equations (A 1)–(A 2) with $z=\eta(\xi_1,\xi_2,\ldots,\xi_\kappa;q)$, then equating like powers of q, we have the mth-order deformation equations

$$\bar{\mathcal{L}}[\phi_m] = c_0\Delta^{\phi}_{m-1}(\xi_1,\xi_2,\ldots,\xi_\kappa)-\bar{S}_m(\xi_1,\xi_2,\ldots,\xi_\kappa)+\chi_m S_{m-1}(\xi_1,\xi_2,\ldots,\xi_\kappa), \tag{A 9}$$

$$\eta_m = c_0\Delta^{\eta}_{m-1}(\xi_1,\xi_2,\ldots,\xi_\kappa)+\chi_m\eta_{m-1}(\xi_1,\xi_2,\ldots,\xi_\kappa), \tag{A 10}$$

The expressions for Δ^{ϕ}_{m-1}, $\bar{S}_m$, S_{m-1} and Δ^{η}_{m-1} are extensions of the definitions in appendix A in Xu *et al.* (2012) from two to κ primary wave components. The linear operator $\bar{\mathcal{L}}$ is defined by

$$\bar{\mathcal{L}}[\phi_m]=\left(\sum_{i=1}^{\kappa}\sum_{j=1}^{\kappa}\omega_i\omega_j\frac{\partial^2\phi_m}{\partial\xi_i\partial\xi_j}+g\frac{\partial\phi_m}{\partial z}\right)\bigg|_{z=0}, \tag{A 11}$$

with the property

$$\bar{\mathcal{L}}^{-1}[\sin(m_1\xi_1+m_2\xi_2+\cdots+m_\kappa\xi_\kappa)]=\frac{\Psi_{m_1,m_2,\ldots,m_\kappa}}{\lambda_{m_1,m_2,\ldots,m_\kappa}},\quad \lambda_{m_1,m_2,\ldots,m_\kappa}\neq 0, \tag{A 12}$$

where

$$\lambda_{m_1,m_2,\ldots,m_\kappa}=g\left|\sum_{i=1}^{\kappa}m_i\boldsymbol{k}_i\right|-\left(\sum_{i=1}^{\kappa}m_i\omega_i\right)^2. \tag{A 13}$$

Up to the mth order, all terms on the right-hand sides of (A 9) and (A 10) are already known, so η_m can be directly expressed by (A 10), and the special solution for ϕ_m is

$$\phi^*_m=\bar{\mathcal{L}}^{-1}[c_0\Delta^{\phi}_{m-1}-\bar{S}_m+\chi_m S_{m-1}]. \tag{A 14}$$

When l resonant wave components ($\boldsymbol{k}_{0,1}$, $\boldsymbol{k}_{0,2}$, …, $\boldsymbol{k}_{0,l}$) are generated by κ primary wave components ($\boldsymbol{k}_1$, $\boldsymbol{k}_2$, …, $\boldsymbol{k}_\kappa$), the corresponding resonance conditions are

$$\begin{cases} m_{\iota,1}\boldsymbol{k}_1+m_{\iota,2}\boldsymbol{k}_2+\cdots+m_{\iota,\kappa}\boldsymbol{k}_\kappa+\boldsymbol{k}_{0,\iota}=0,\\ m_{\iota,1}\omega_1+m_{\iota,2}\omega_2+\cdots+m_{\iota,\kappa}\omega_\kappa+\omega_{0,\iota}=0,\end{cases}\quad \iota=1,2,\ldots,l \tag{A 15}$$

or alternatively

$$g\left|\sum_{i=1}^{\kappa}m_{\iota,i}\boldsymbol{k}_i\right|=\left(\sum_{i=1}^{\kappa}m_{\iota,i}\omega_i\right)^2, \tag{A 16}$$

where the linear frequency $\omega_{0,\iota}=\sqrt{g|\boldsymbol{k}_{0,\iota}|}$ is applied. It is worth mentioning that the resonance conditions (A 16) (or (A 15)) are a special case of $\lambda_{m_1,m_2,\ldots,m_\kappa}$, defined in

(A 13), equal to zero. Besides, owing to the definition of $\lambda_{m_1,m_2,\ldots,m_\kappa}$, it holds that $\lambda_{1,0,0,\ldots} \equiv 0$, $\lambda_{0,1,0,\ldots} \equiv 0$, $\ldots$ and $\lambda_{0,0,\ldots,1} \equiv 0$ all the time. In other words, there are $\kappa + l$ zero eigenvalues of $\lambda_{m_1,m_2,\ldots,m_\kappa}$ when the resonance condition is exactly satisfied. Thus, from a mathematical viewpoint, the common solution of ϕ_m reads

$$\phi_m = \phi_m^* + A_{m,1}\Psi_{1,0,\ldots,0} + A_{m,2}\Psi_{0,1,\ldots,0} + \cdots + A_{m,\kappa}\Psi_{0,0,\ldots,1} + \sum_{i=1}^{l} A_{m,\kappa+i}\Psi_i^*, \tag{A 17}$$

where ϕ_m^* is the special solution of ϕ_m defined in (A 14), Ψ_i^* is the eigenfunction related to resonant wave components and $A_{m,i}$ is a constant to be determined.

According to the definition of (A 12), there should be no terms of $\sin(m_1\xi_1 + m_2\xi_2 + \cdots + m_\kappa\xi_\kappa)$ related to $\lambda_{m_1,m_2,\ldots,m_\kappa} = 0$ appearing on the right-hand side of (A 9), otherwise secular terms are generated. So in order to avoid secular terms in the first-order approximation, we choose

$$\eta_0(\xi_1, \xi_2, \ldots, \xi_\kappa) = 0, \tag{A 18}$$

$$\phi_0(\xi_1, \xi_2, \ldots, \xi_\kappa, z) = A_{0,1}\Psi_{1,0,\ldots,0} + A_{0,2}\Psi_{0,1,\ldots,0} + \cdots + A_{0,\kappa}\Psi_{0,0,\ldots,1} + \sum_{i=1}^{l} A_{0,\kappa+i}\Psi_i^*. \tag{A 19}$$

Here, the coefficients $A_{0,i}$ are unknown constants determined by avoiding the secular terms in the first-order approximation.

Note that regardless of whether the order of the resonant wave components is the same as that of the primary ones or not, we consider them both in the initial guess (A 19). This relies on there being no dependence on small/large physical parameters in HAM, in which the transfer of the original nonlinear PDEs to an infinite number of linear subproblems does not need to consider the orders of different wave components.

Appendix B. Solution procedure of the collocation method

For simplicity, we consider the steady-state resonance waves caused only by two primary wave components. It is believed that the procedure described below can be easily extended to the case of multiple primary wave components. According to the solution expression (2.12), the velocity potential ϕ is expressed as follows:

$$\phi = \sum_{m=1}^{N}\sum_{n=-N}^{N} C_{m,n}^{\phi}\Psi_{m,n} + \sum_{n=1}^{N} C_{0,n}^{\phi}\Psi_{0,n}, \tag{B 1}$$

where $N = 17$ is the maximum order of expansion. Considering the symmetry condition $\phi(\xi_1, \xi_2, z) = -\phi(2\pi - \xi_1, 2\pi - \xi_2, z)$, the collocation points are selected as

$$\xi_{1,i} = \frac{i-1}{N+1}\pi, \quad i = 2, 3, \ldots, N+1, \tag{B 2}$$

$$\xi_{2,j} = \frac{j-1}{N+\frac{1}{2}}\pi, \quad j = 1, 2, \ldots, 2N+1, \tag{B 3}$$

together with

$$\xi_{2,j} = \frac{j-1}{N}\pi, \quad j = 1, 2, \ldots, N \quad \text{for } \xi_1 = 0. \tag{B 4}$$

The ξ_2 derivative of the kinematic condition (2.7) is used instead of the original equation at $\xi_1 = \xi_2 = 0$, as the kinematic condition (2.7) becomes trivial when $\xi_1 = \xi_2 = 0$. Substituting (B 1) into (2.7) and (2.8) and the above collocation points into ξ_1 and ξ_2 in them, we obtain $2N(2N + 2)$ equations for $2N(2N + 2)$ unknown quantities: $C^{\phi}_{m,n}$ and $\eta(\xi_{1,i}, \xi_{2,j})$.

The $2N(2N + 2)$ nonlinear equations are solved by the Newton method. The iteration stops when the differences of unknown quantities before and after an iteration is smaller than 10^{-12}. The fifth-order approximation provided by HAM is the initial solution of the iteration. Then, the initial solution for another solution at a slightly different set of parameters comes from the previous solution, provided the values of the two sets of parameters are close enough. For more details, please refer to Okamura (1996).

Appendix C. Detailed mathematical formulas for (5.23)

We have

$$\sum_{J=-N}^{N}\sum_{K=-N}^{N} R^{(1)}_{JK} a_{JK} + \sum_{J=-N}^{N}\sum_{K=-N}^{N} S^{(1)}_{JK} b_{JK} = \mathrm{i}\sigma \sum_{J=-N}^{N}\sum_{K=-N}^{N} T^{(1)}_{JK} a_{JK}, \tag{C 1}$$

$$\sum_{J=-N}^{N}\sum_{K=-N}^{N} R^{(2)}_{JK} a_{JK} + \sum_{J=-N}^{N}\sum_{K=-N}^{N} S^{(2)}_{JK} b_{JK} = \mathrm{i}\sigma \sum_{J=-N}^{N}\sum_{K=-N}^{N} T^{(2)}_{JK} b_{JK}, \tag{C 2}$$

where

$$R^{(1)}_{JK} = \{R_4 + \mathrm{i}(p' + J)R_1 + \mathrm{i}(q' + K)R_2\}\mathrm{e}^{\mathrm{i}(J\xi_1 + K\xi_2)}, \tag{C 3}$$

$$S^{(1)}_{JK} = \{\mathrm{i}(p' + J)R_5 + \mathrm{i}(q' + K)R_6 - \kappa_{JK}\}\mathrm{e}^{\mathrm{i}(J\xi_1 + K\xi_2)}\mathrm{e}^{\kappa_{JK}\bar{\eta}}, \tag{C 4}$$

$$T^{(1)}_{JK} = \mathrm{e}^{\mathrm{i}(J\xi_1 + K\xi_2)}, \tag{C 5}$$

$$R^{(2)}_{JK} = R_3\mathrm{e}^{\mathrm{i}(J\xi_1 + K\xi_2)}, \tag{C 6}$$

$$S^{(2)}_{JK} = \{\mathrm{i}(p' + J)R_1 + \mathrm{i}(q' + K)R_2 + \kappa_{JK}\bar{\phi}_z\}\mathrm{e}^{\mathrm{i}(J\xi_1 + K\xi_2)}\mathrm{e}^{\kappa_{JK}\bar{\eta}}, \tag{C 7}$$

$$T^{(2)}_{JK} = \mathrm{e}^{\mathrm{i}(J\xi_1 + K\xi_2)}\mathrm{e}^{\kappa_{JK}\bar{\eta}}. \tag{C 8}$$

REFERENCES

Annenkov, S. Y. & Shrira, V. I. 2006 Role of non-resonant interactions in the evolution of nonlinear random water wave fields. *J. Fluid Mech.* **561**, 181–208.

Badulin, S. I., Shrira, V., Kharif, C. & Ioualalen, M. 1995 On two approaches to the problem of instability of short-crested water waves. *J. Fluid Mech.* **303** (1), 297–326.

Benjamin, T. B. & Brooke, F. J. 1967 The disintegration of wave trains on deep water. *J. Fluid Mech.* **27** (3), 417–430.

Benney, D. J. 1962 Non-linear gravity wave interactions. *J. Fluid Mech.* **14** (4), 577–584.

Bretherton, F. P. 1964 Resonant interactions between waves. The case of discrete oscillations. *J. Fluid Mech.* **20** (3), 457–479.

Chen, B & Saffman, P. G. 1978 Steady gravity–capillary waves on deep water. I. Weakly nonlinear waves. Tech. Rep. DTIC Document.

Craik, A. D. D. 1985 *Wave interactions and fluid flows*. Cambridge University Press.

Dias, F. & Kharif, C. 1999 Nonlinear gravity and capillary–gravity waves. *Annu. Rev. Fluid Mech.* **31** (1), 301–346.

FRANCIUS, M. & KHARIF, C. 2006 Three-dimensional instabilities of periodic gravity waves in shallow water. *J. Fluid Mech.* **561** (1), 417–437.

FRUCTUS, D., KHARIF, C., FRANCIUS, M., KRISTIANSEN, O., CLAMOND, D. & GRUE, J. 2005 Dynamics of crescent water wave patterns. *J. Fluid Mech.* **537**, 155–186.

GRIMSHAW, R. 2005 *Nonlinear Waves in Fluids: Recent Advances and Modern Applications*. Springer.

HAMMACK, J. L. & HENDERSON, D. M. 1993 Resonant interactions among surface water waves. *Annu. Rev. Fluid Mech.* **25** (1), 55–97.

HASSELMANN, K. 1962 On the non-linear energy transfer in a gravity-wave spectrum. *J. Fluid Mech.* **12**, 481–500.

HASSELMANN, K. 1963*a* On the non-linear energy transfer in a gravity-wave spectrum. Part 2. Conservation theorems; wave–particle analogy; irreversibility. *J. Fluid Mech.* **15** (2), 273–281.

HASSELMANN, K. 1963*b* On the non-linear energy transfer in a gravity-wave spectrum. Part 3. Evaluation of the energy flux and swell–sea interaction for a Neumann spectrum. *J. Fluid Mech.* **15** (3), 385–398.

IOUALALEN, M. & KHARIF, C. 1993 Stability of three-dimensional progressive gravity waves on deep water to superharmonic disturbances. *Eur. J. Mech. Fluids* B **12** (3), 401–414.

IOUALALEN, M. & KHARIF, C. 1994 On the subharmonic instabilities of steady three-dimensional deep water waves. *J. Fluid Mech.* **262**, 265–265.

JANSSEN, P. A. E. M. 2003 Nonlinear four-wave interactions and freak waves. *J. Phys. Oceanogr.* **33** (4), 863–884.

KARTASHOVA, E. 2010 *Nonlinear resonance analysis: theory, computation, applications*. Cambridge University Press.

KOMEN, G. J., CAVALERI, L., DONELAN, M., HASSELMANN, K., HASSELMANN, S. & JANSSEN, P. A. E. M. 1996 *Dynamics and modelling of ocean waves*. Cambridge University Press.

LIAO, S. J. 1992 Proposed homotopy analysis techniques for the solution of nonlinear problems. PhD thesis, Shanghai Jiao Tong University.

LIAO, S. J. 2003 *Beyond Perturbation: Introduction to the Homotopy Analysis Method*. Chapman & Hall/CRC Press.

LIAO, S. J. 2011 On the homotopy multiple-variable method and its applications in the interactions of nonlinear gravity waves. *Commun. Nonlinear Sci. Numer. Simul.* **16** (3), 1274–1303.

LIAO, S. J. 2012 *Homotopy Analysis Method in Nonlinear Differential Equations*. Springer & Higher Education Press.

LIAO, S. J. 2013 *Advances in Homotopy Analysis Method*. World Scientific Press.

LONGUET-HIGGINS, M. S. 1962 Resonant interactions between two trains of gravity waves. *J. Fluid Mech.* **12** (3), 321–332.

LONGUET-HIGGINS, M. S. & SMITH, N. D. 1966 An experiment on third-order resonant wave interactions. *J. Fluid Mech.* **25** (3), 417–435.

MACKAY, R. S. & SAFFMAN, P. G. 1986 Stability of water waves. *Proc. R. Soc. Lond.* A **406** (1830), 115–125.

MADSEN, P. A. & FUHRMAN, D. R. 2006 Third-order theory for bichromatic bi-directional water waves. *J. Fluid Mech.* **557**, 369–397.

MCGOLDRICK, L. F., PHILLIPS, O. M., HUANG, N. E. & HODGSON, T. H. 1966 Measurements of third-order resonant wave interactions. *J. Fluid Mech.* **25** (3), 437–456.

MCLEAN, J. W. 1982 Instabilities of finite-amplitude water waves. *J. Fluid Mech.* **114** (1), 315–330.

OKAMURA, M. 1996 Notes on short-crested waves in deep water. *J. Phys. Soc. Japan* **65** (9), 2841–2845.

PHILLIPS, O. M. 1960 On the dynamics of unsteady gravity waves of finite amplitude. *J. Fluid Mech.* **9**, 193–217.

PHILLIPS, O. M. 1977 *The Dynamics of the Upper Ocean*. Cambridge University Press.

PHILLIPS, O. M. 1981 Wave interactions – the evolution of an idea. *J. Fluid Mech.* **106** (1), 215–227.

ROBERTS, A. J. 1983 Highly nonlinear short-crested water waves. *J. Fluid Mech.* **135**, 301–321.

SHRIRA, V. I., BADULIN, S. I. & KHARIF, C. 1996 A model of water wave 'horse-shoe' patterns. *J. Fluid Mech.* **318**, 375–405.

XU, D., LIN, Z., LIAO, S. & STIASSNIE, M. 2012 On the steady-state fully resonant progressive waves in water of finite depth. *J. Fluid Mech.* **710**, 379–418.

YOUNG, I. R. 1999 *Wind Generated Ocean Waves*. vol. 2. Elsevier.

YUEN, H. C. & LAKE, B. M. 1982 Nonlinear dynamics of deep-water gravity waves. *Adv. Appl. Mech.* **22**, 67–229.

ZAKHAROV, V. E. 1968 Stability of periodic waves of finite amplitude on the surface of a deep fluid. *J. Appl. Mech. Tech. Phys.* **9** (2), 190–194.